Brain and Behavior

Open Access

# Immunofluorescent spectral analysis reveals the intrathecal cannabinoid agonist, AM1241, produces spinal anti-inflammatory cytokine responses in neuropathic rats exhibiting relief from allodynia

Jenny L. Wilkerson[1], Katherine R. Gentry[2], Ellen C. Dengler[1], James A. Wallace[1], Audra A. Kerwin[1], Megan N. Kuhn[1], Alexander M. Zvonok[3], Ganesh A. Thakur[3], Alexandros Makriyannis[3] & Erin D. Milligan[1]

[1]Department of Neurosciences, Health Sciences Center, School of Medicine, University of New Mexico, Albuquerque, New Mexico 87131
[2]Department of Anesthesiology and Critical Care Medicine, Health Sciences Center, School of Medicine, University of New Mexico, Albuquerque, New Mexico 87131
[3]Center for Drug Discovery, Northeastern University, Boston, Massachusetts 02115

**Keywords**
CCI, DRG, MAGL, pain, paraffin immunohistochemistry.

**Correspondence**
Jenny L. Wilkerson and Erin D. Milligan, Department of Neurosciences, University of New Mexico, HSC, MSC08-4740, 1 University of New Mexico, Albuquerque, NM 87131.
Tel: +1(505) 272-4441; Fax: +1(505) 272-8082;
E-mail: JLWilkerson@salud.unm.edu; EMilligan@salud.unm.edu

Funded by NIH grants: NIDA 018156, GM60201 and also funded in part by the Dedicated Health Research Funds from the University of New Mexico School of Medicine.

Received: 2 August 2011; Accepted: 30 January 2012

doi: 10.1002/brb3.44

## Abstract

During pathological pain, the actions of the endocannabinoid system, including the cannabinoid 2 receptor ($CB_2R$), leads to effective anti-allodynia and modifies a variety of spinal microglial and astrocyte responses. Here, following spinal administration of the $CB_2R$ compound, AM1241, we examined immunoreactive alterations in markers for activated p38 mitogen-activated protein kinase, interleukin-1$\beta$ (IL-1$\beta$), the anti-inflammatory cytokine, interleukin-10 (IL-10) as well as degradative endocannabinoid enzymes, and markers for altered glial responses in neuropathic rats. In these studies, the dorsal horn of the spinal cord and dorsal root ganglia were examined. AM1241 produced profound anti-allodynia with corresponding immunoreactive levels of p38 mitogen-activated kinase, IL-1$\beta$, IL-10, the endocannabinoid enzyme monoacylglycerol lipase, and astrocyte activation markers that were similar to nonneuropathic controls. In contrast, spinal AM1241 did not suppress the increased microglial responses observed in neuropathic rats. The differences in fluorescent markers were determined within discrete anatomical regions by applying spectral analysis methods, which virtually eliminated nonspecific signal during the quantification of specific immunofluorescent intensity. These data reveal expression profiles that support the actions of intrathecal AM1241 control pathological pain through anti-inflammatory mechanisms by modulating critical glial factors, and additionally decrease expression levels of endocannabinoid degradative enzymes.

## Introduction

Microglia and astrocytes (glia) play a crucial role in the development and maintenance of chronic neuropathic pain in various animal models (DeLeo et al. 2007). Increased glial activation is well known to occur in the dorsal horn of the spinal cord in animal models of peripheral neuropathy, as demonstrated by increased production of glial fibriliary acidic protein (GFAP) in astrocytes and ionized calcium binding adaptor molecule-1 (Iba-1) in microglia (Pekny and Pekna 2004; Racz et al. 2008b). When strongly activated, glia can increase expression of proinflammatory factors such as phosphorylated p38 mitogen-activated protein kinase (p-p38MAPK) that can lead to production and release of proinflammatory cytokines such as interleukin-1$\beta$ (IL-1$\beta$) and tumor necrosis factor-$\alpha$ (TNF-$\alpha$), which subsequently bind and activate their respective receptors on nearby neurons and glia (De Leo et al. 2006; Watkins et al. 2007; Milligan and Watkins 2009). The cellular anatomical localization of p-p38MAPK is predominantly expressed and is functionally important in

spinal cord microglia and corresponding satellite cells in dorsal root ganglia (DRG) during neuropathic pain (Schafers et al. 2003; Svensson et al. 2005b; Boyle et al. 2006; Ji and Suter 2007; Sorkin et al. 2009). IL-1$\beta$ mRNA and protein are upregulated within spinal cord homogenates of rats with pathological pain (Holguin et al. 2004). However, immunohistochemical detection of increased IL-1$\beta$ protein, as well as alterations in the anti-inflammatory cytokine, interleukin-10 (IL-10), in intact spinal cord dorsal horn from rats with peripheral neuropathy has not yet been characterized. One goal of these studies is to quantify immunoreactivity (IR) for IL-1$\beta$ as well as IL-10 in sections of the intact dorsal horn from rats with chronic peripheral neuropathy. In addition, changes in immunoreactive p-p38MAPK levels were examined to verify prior reports that increase in p-p38MAPK occurs in combination with increased proinflammatory cytokine expression. Peripheral neuropathy is assessed by the presence of allodynia, characterized as a sensitivity to light mechanical touch that is not present under healthy conditions.

AM1241 is a widely characterized cannabinoid agonist that controls hyperalgesia (exaggerated nociceptive thresholds) and allodynia following intraperitoneal (i.p.) (Ibrahim et al. 2006; Rahn et al. 2008), intravenous (i.v.) (Beltramo et al. 2006), intra-DRG, or intrathecal (i.t.) (Hsieh et al. 2011) injection. In the current studies, we sought to determine the timecourse and dose-dependent changes in allodynia produced by unilateral chronic constriction injury (CCI) of the rat sciatic nerve following i.t. AM1241 administration to avoid known peripheral actions of the compound. The development of bilateral allodynia following unilateral CCI has been documented in numerous studies (Paulson et al. 2000, 2002; Milligan et al. 2006, 2007; Loram et al. 2009). We therefore followed not only bilateral sensory behavioral changes, but also quantitative changes in the bilateral IR of: (1) cytokines, (2) p-p38MAPK, (3) enzymes responsible for the bioavailability of endocannabinoids characterized to exert analgesic properties (Kinsey et al. 2009, 2010), and (4) markers reflecting changes in astrocytic and microglial responses in spinal cord and DRG.

Existing evidence shows that AM1241 acts as an agonist at the cannabinoid 2 receptor ($CB_2R$) that results in suppression of nociceptive responses (Rahn et al. 2010), and prevents neuropathic and inflammatory pain (Nackley et al. 2004; Beltramo et al. 2006; Rahn et al. 2008), with selectivity demonstrated not only by utilizing pharmacological $CB_2R$ antagonists, but also by examining AM1241 analgesic efficacy in $CB_2R$ knockout mice (Ibrahim et al. 2003, 2006). $CB_2Rs$ are characterized on microglia and macrophages in cell culture (Walter et al. 2003; Cabral and Marciano–Cabral 2005; Ehrhart et al. 2005) and in the rodent spinal cord following peripheral nerve damage (Zhang et al. 2003; Romero-Sandoval et al. 2008a) or in transgenic mice overexpressing the $CB_2R$ (Racz et al. 2008b), as well as in the human central nervous system (CNS) under inflammatory diseased conditions (Nunez et al. 2008). Given that AM1241 can act on $CB_2Rs$ expressed on spinal microglia, the potential additional (1) cytokine and (2) p-p38MAPK involvement in AM1241s efficacy in producing spinal anti-inflammatory actions concurrent with anti-allodynia were examined in these studies.

Related to these goals, we examined two methods to analyze immunofluorescent images of spinal cord tissue sections to identify the most sensitive procedure for detecting and quantifying differences in specific immunoreactive protein markers. In this context, an alternative method that utilizes spectral analysis procedures, demonstrated here, can be advantageous over conventional methods of image analysis.

## Materials and Methods

### Animals

A total of 52 pathogen-free adult male Sprague Dawley rats (300–400 g; Harlan Labs, Madison, WI) were used in all experiments. Rats were double housed in a temperature- and light-controlled (12 h light/dark; lights on at 6:00 AM) environment, with standard rodent chow and water available ad libitum. All procedures were approved by the Institutional Animal Care and Use Committee (IACUC) of the University of New Mexico Health Sciences Center.

### Drugs

The $CB_2R$ agonist used in these experiments was (R,S)-(2-iodo-5-nitrophenyl)-(1-[(1-methylpiperidin-2-yl)methyl]-1*H*-indol-3yl)-methanone (AM1241) from the aminoalkyndole classification (Yao et al. 2006). Water-soluble hydrochloride salt of racemic AM1241 was generously gifted (A. Makriyannis, Center for Drug Discovery, Northeastern University). Initial doses of AM1241 were based on those previously reported for i.v. injection (Beltramo et al. 2006) and pilot studies. A 1000-fold dose range of AM1241, dissolved in sterile saline (Hospira Inc, Lake Forest, IL) was tested (10–0.01 $\mu$g in 10 $\mu$l) or equivolume sterile saline as vehicle. Of note, fully solubilized AM1241 resulted in a clear solution.

### Behavioral assessment of allodynia

Baseline (BL) responses to light mechanical touch were assessed using the von Frey test after animals were habituated to the testing environment, as previously described (Chaplan et al. 1994; Milligan et al. 2000). Briefly, rats were placed atop 2-mm bars with 8-mm spacing between parallel bars for approximately 45 min for five days. All behavioral testing was performed during the first half of the light cycle in a sound-, light-, and temperature-controlled room. The von Frey test

utilizes a series of calibrated monofilaments (3.61–5.18 log stimulus intensity; North Coast Medical, Morgan Hills, CA), applied randomly to the left and right plantar surface of the hindpaw for 8 sec. Lifting, licking, or shaking the paw was considered a response. Following CCI or sham surgery, animals were behaviorally tested on Day 3 and 10. On Day 10 post-surgery after behavioral assessment, all animals received an i.t. AM1241 or vehicle injection followed by behavioral reassessment at 30 min intervals for 5 h and again at 24 h. Testing was performed in a blinded fashion.

## CCI surgery

Following BL behavioral assessment, the surgical procedure for chronic constriction of the sciatic nerve was completed as previously described (Bennett and Xie 1988). Briefly, isoflurane (induction 5% volume followed by 2.5% in oxygen), anesthetized rats had their mid-to-lower back and the dorsal left thigh shaved and cleaned with diluted Bacti-Stat AE, (Eco-Lab HealthCare Division, Mississauga, Ontario, Canada). Using aseptic procedures, the sciatic nerve was carefully isolated and loosely ligated with 4 segments of chromic gut sutures (Ethicon, Somerville, NJ) with each suture approximately 1 mm apart. Sham surgery was identical to CCI surgery but without the nerve ligation. The overlying muscle was sutured closed with two 3–0 sterile silk sutures (Ethicon, Somerville, NJ), and animals recovered from anesthesia within approximately 5 min.

## Intrathecal (i.t.) injection

AM1241 was administered via acute i.t. catheter. Injections were performed as previously described (Milligan et al. 2005b). Briefly, rats were anesthetized with isoflurane and an 18-gauge sterile, hypodermic needle, with the plastic hub removed was inserted between lumbar vertebrae L5 and L6. The PE-10 injection catheter was marked between 7.7 and 7.8 cm from an open end, with the other end inserted into a 30-gauge needle. A sterile Hamilton syringe was fitted with the 30-gauge needle and the attached PE-10 catheter, and collectively referred to as an injection catheter. Either 10 $\mu$l drug or equivolume vehicle was withdrawn from respective vials via the open end of the PE-10 injection catheter, which was gently inserted into the placed 18-gauge needle and threaded rostrally to the 7.7 cm marking on the injection catheter. The resulting position of the inserted tip of the PE-10 catheter occurs at the i.t. lumbosacral enlargement (~L4–L5). During this time, light tail twitching and a small amount of cerebrospinal fluid efflux from the 18-gauge needle was typically observed indicating successful i.t. catheter placement. Drug or vehicle was injected during a 10-sec interval. Upon completion of injection, the PE-10 i.t. catheter was removed followed by removal of the 18-gauge needle. A 100% motor recovery rate was observed from this injection procedure.

## Immunohistochemical procedures

Following behavioral assessment at indicated time points (Figs. 3, 4), animals were overdosed with an i.p. injection (0.8-1.3 cc) of sodium phenobarbital (Sleepaway, Fort Dodge Animal Health, Fort Dodge, IA) and perfused transcardially with saline followed by 4% paraformaldehyde. Whole vertebral columns with intact spinal cord (cervical 2 through sacral 1 spinal column segments) were removed, and underwent overnight fixation in 4% paraformaldehyde at 4°C. This tissue collection procedure ensured that all relevant anatomical components, including the spinal cord, DRG, and related meninges, were intact within the vertebral column, allowing important spatial relationships to be examined for corresponding functional interactions at individual and specific spinal cord levels. All specimens underwent EDTA (Sigma Aldrich, St. Louis, MO) decalcification for 30 days, and spinal cord sections were subsequently paraffin processed and embedded in Paraplast Plus Embedding Media (McCormick Scientific, St. Louis, MO) as previously described (Wallace et al. 1996). Four adjacent tissue sections (7 $\mu$m) were mounted on a vectabond-treated slide (Vector Labs, Burlingame, CA), and allowed to adhere to the slide overnight at 40°C.

Approximately 130 slides per L4–L6 lumbar spinal cord, and 40 slides per lumbar L5 DRG, were generated in this manner for each animal. Two slides from an animal's lumbar spinal cord and two slides of DRG were randomly chosen for each staining procedure. The 7-$\mu$m sections then underwent deparaffinization, and rehydration via descending alcohols to phosphate buffered saline (PBS) (1×, pH 7.4). Sections were then processed with microwave antigen retrieval procedures (citrate buffer pH 6.0, or tris-based buffer, pH 9.0; BioCare Medical, Concord, CA).

## Antibody staining

Slides were incubated with 5% normal donkey serum (NDS), in PBS (1×, pH 7.4) for 2 h, followed by overnight primary antibody (Table 1) incubation in a humidity chamber at 3°C. Slides underwent secondary antibody incubation (Table 1) for 2 h in a humidity chamber at room temperature, rinsed in PBS, and then coverslipped with Vectashield containing the nuclear stain 4′,6-diamidino-2-phenylindole (DAPI) (Vector Labs, Burlingame, CA). For detection of monoacylglycerol lipase (MAGL), phosphorylated p38MAPK, and IL-10 protein, sections were incubated overnight with primary antibodies, incubated with biotinylated secondary antibody (Table 1) for 1 h, and then treated with Vectastain ABC Elite kit (Vector Labs, Burlingame, CA) and stained using TSA Plus

 

**Table 1.** List of all antibodies used in this study and designated under the appropriate column heading. Primary antibodies for polyclonal GFAP (astrocyte-specific glial fibriliary acidic protein, Millipore, Billerica, MA) previously used in other studies (Wu et al. 2002; Fukudome et al. 2003), monoclonal GFAP (astrocyte-specific GFAP, Progen, Heidelberg, Germany) previously used in other studies (Achstatter et al. 1986), Iba-1 (microglia, monocyte-specific calcium channel protein, Wako Chemicals, Osaka, Japan) previously used in other studies (Imai et al. 1996; Ohsawa et al. 2000), FAAH (fatty acid amide hydrolase, endocannabinoid degradative enzyme, Cayman Chemicals, Ann Arbor, MI) previously used in other studies (Yasuo et al.; Starowicz et al. 2008), IL-1$\beta$ protein (proinflammatory cytokine, Santa Cruz Biotechnology, Santa Cruz, CA) previously used in other studies (Bellucci et al. 2004; Reed et al. 2009), MAGL (monoacylglyerol lipase, endocannabinoid degradative enzyme, Abcam, Cambridge, MA) previously used in other studies (Marquez et al. 2009), phosphorylated p38MAPK (activated proinflammatory cytokine signaling pathway, Cell Signaling Technology, Beverly, MA) previously used in other studies (Schafers et al. 2003), and IL-10 protein (anti-inflammatory cytokine, R & D Systems, Minneapolis, MN) previously used in other studies (Thompson–Snipes et al. 1991; Hor et al. 2004) were used. Secondary antibody incubation was performed with the indicated fluorophore-conjugated secondary antibody. For MAGL, phosphorylated p38MAPK, and IL-10 protein, after overnight primary incubation, sections were instead incubated with biotinylated secondary antibody.

| Primary antibody | Antibody clone | Indication | Anatomical region | Vendor/ Catolog number | Host | Dilution used | Antigen retrieval | TSA used | Secondary antibody[1] |
|---|---|---|---|---|---|---|---|---|---|
| GFAP | Polyclonal | Astrocyte | Dorsal horn spinal cord | Millipore/AB5804 | Rabbit | 1:1000 | Tris buffer | No | Rhodamine Red Donkey anti-Rabbit (1:200) |
| GFAP | Monoclonal | Satellite cell | DRG | Progen/65011 | Rabbit | 1:10 | Citrate buffer | No | Rhodamine Red Donkey anti-Rabbit (1:200) |
| Iba-1 | Polyclonal | Microglia | Dorsal horn spinal cord | Wako/019–19741 | Rabbit | 1:300 | Tris buffer | No | Rhodamine Red Donkey anti-Rabbit (1:200) |
| FAAH | Polyclonal | Ecb enzyme | Dorsal horn spinal cord | Cayman Chemical/101600 | Rabbit | 1:100 | Tris buffer | No | Rhodamine Red Donkey anti-Rabbit (1:200) |
| MAGL | Polyclonal | Ecb enzyme | Dorsal horn spinal cord | Abcam/ AB24701 | Rabbit | 1:100 | Citrate buffer | Yes | Biotinylated Donkey anti-Rabbit (1:1300) |
| p-p38 | Polyclonal | Phospho-p38 MAP Kinase | Dorsal horn spinal cord, DRG | Cell Signaling/45112 | Rabbit | 1:800 | Citrate buffer | Yes | Biotinylated Donkey anti-Rabbit (1:1300) |
| IL-10 | Polyclonal | IL-10 protein | Dorsal horn spinal cord, DRG | R & D Systems/ AF519 | Goat | 1:250 | Citrate buffer | Yes | Biotinylated Donkey anti-Goat (1:1300) |
| IL-1$\beta$ | Polyclonal | IL-1$\beta$ protein | Dorsal horn spinal cord, DRG | Santa Cruz/SC-7884 | Rabbit | 1:300 | Tris buffer | No | FITC, Rhodamine Red Donkey anti-Rabbit (1:200) |

[1]All secondary antibodies are from Jackson Immunoresearch (West Grove, PA).

Fluorescein System (PerkinElmer Life Sciences, Waltham, MA) and finally coverslipped with Vectashield containing DAPI. Stained section orientation was kept consistent throughout for proper identification of ipsilateral and contralateral spinal cord and DRGs. For lumbar spinal cord, sections were taken from L4–L6 and the dorsal horn analyzed (Fig. 1A). For DRG material, sections were taken containing the DRG with the projection to L5, and the most distal portion of the DRG was analyzed (Fig. 1B). Low-magnification photomicrographs were obtained (Fig. 1A and 1B) using a Nikon Optiphot fluorescent microscope equipped with a DP2-BSW (Olympus) camera.

## Immunohistochemical image analysis

### *Image J software analysis*

Fluorescent images for standard fluorescence analysis were obtained in the same manner as detailed above, with DAPI omitted from the Vectasheild mounting media. This was to ensure that DAPI staining did not potentially obscure the fluorescence intensity. Images were taken on an Olympus BX51 microscope (Center Valley, PA) equipped with an Olympus DP72 camera. Images were then converted to gray scale and analyzed using Image J software available for free download at http://rsb.info.nih.gov/ij/. Briefly, an outline of the dorsal horn gray matter was drawn on an image, and holding the area within this outline consistent, the fluorescent intensity was obtained within this area for each image. This value was generated for each given tissue section (e.g., ipsilateral dorsal horn spinal cord) and averaged together (total of four tissue sections from a single animal) for an overall value. Therefore, for each anatomical location (e.g., ipsilateral and contralateral dorsal horn spinal cord and DRG), the four values (fluorescent intensity average count/sec/mm$^2$) were averaged to obtain an individual animal's overall fluorescent intensity, with three animals in each experimental

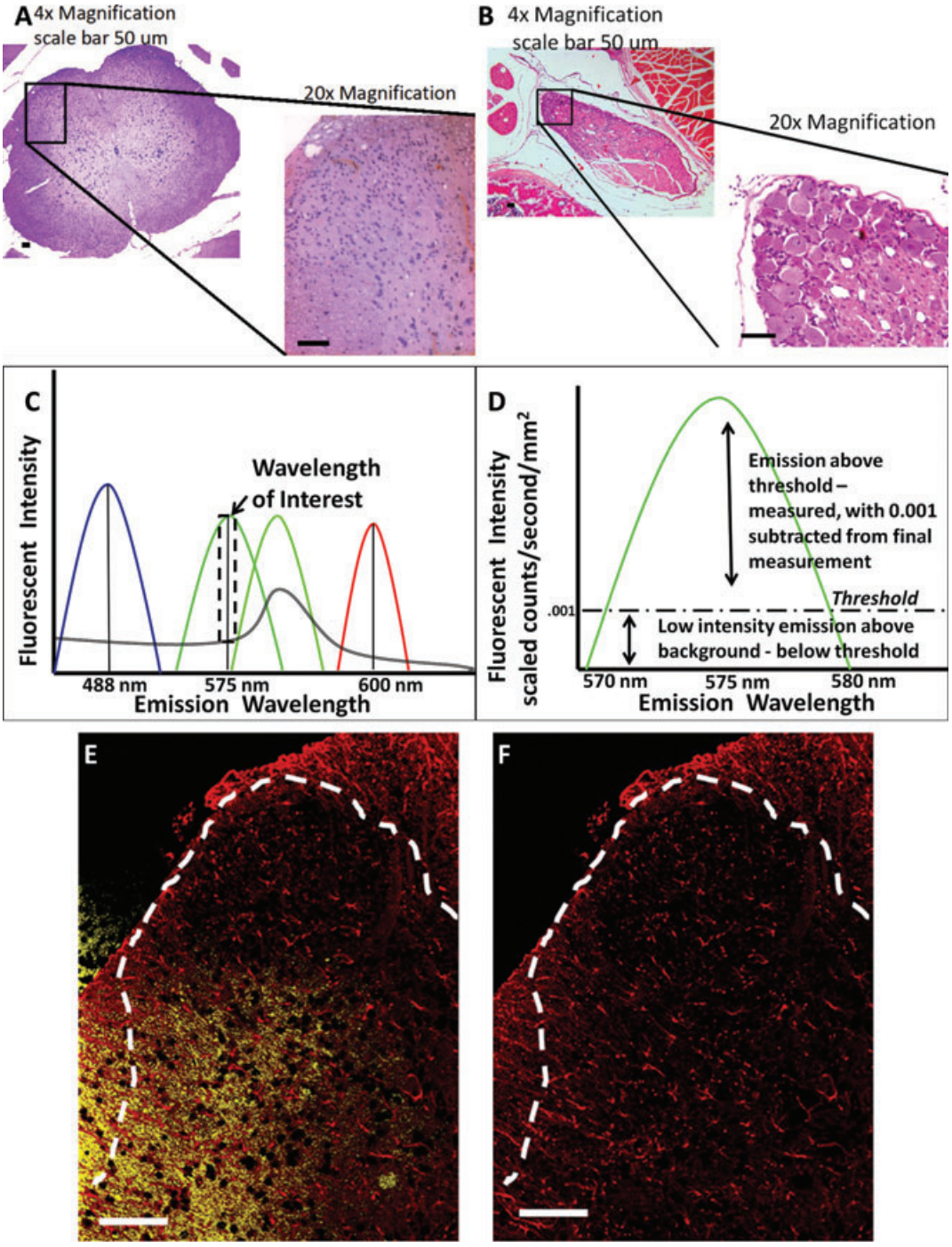


**Figure 1.** Anatomical location of images acquired and spectral analysis allows for discrete fluorescence signal detection and analysis. (**A**) Hematoxylin and eosin staining of the dorsal horn of the spinal cord and (**B**) dorsal root ganglion (area within black box) is displayed in context to relevant anatomical structures (the entire spinal cord and partial cauda equina, respectively) at 4× magnification, and then at 20× magnification. (**C**) Representative fluorescent emission for DAPI (blue) FITC (light green), GFP (dark green) Rhodamine Red (red), and autofluorescence (double black). Selection of narrow fluorescent peak emission bands (dotted black box around FITC wavelength) allows for analysis of only FITC signal, without autoflourescent or GFP signal contaminating fluorescent analysis. (**D**) Representative fluorescent emission threshold level of FITC defined and expanded from dotted black box in (**C**) with the fluorescent threshold of intensity set (dashed black line), above autofluorescent levels. (**E**) Representative spectral image of dorsal horn spinal cord as stained for GFAP (red), with autofluorescent signal defined in yellow. (**F**) Same image in (**E**) with autofluorescent signal removed. In all images the scale bar is equal to 50 $\mu$m.

treatment group, to generate an average for that experimental condition. Likewise, background values were generated from control tissues incubated with PBS and the given secondary antibody, and averaged together. The average background was then subtracted from the above-mentioned average of each experimental treatment group.

### *Spectral analysis of images*

All images of the spinal cord dorsal horn and DRGs were captured by a Zeiss Axioscope Microscope at 20× magnification with a Nuance Spectral Camera (Cambridge Research & Instrumentation, Woburn, MA). Utilizing the Nuance computer software, the fluorescent wavelength emission spectra was initially determined for each fluorophore utilized in the detection of the primary antibody of interest (DAPI, 488 ± 10 nm; FITC, 575 ± 5 nm; Rhodamine Red 600 ± 5 nm) by using a control slide with only a drop of the pure fluorophore. This was performed in the absence of a tissue specimen that may potentially obscure the measurement of the fluorophore's emission spectra. Two sets of additional control slides with tissue sections, one with only PBS without primary but with secondary antibody treatment, and the other, with primary but without secondary antibody treatment, were then used to objectively eliminate low-intensity fluorescence and autofluorescence background "noise" from our measurements (Fig. 1C). Using control slides, the Nuance software allows the user to set an acceptable threshold of low-level emission fluorescent intensity (as opposed to the software's "autothreshold" option) within and outside the defined wavelength of interest between tissue samples. The experimenter determined low-level emission intensity by closely replicating the composite computer image with that observed through the eyepiece. Emission values that fall below this acceptable threshold of low-level emission, within and outside the defined wavelength of interest, were eliminated from our measurements (Fig. 1D). This level of fluorescent threshold for each protein marker was determined by the user, finding the most appropriate wavelength of interest that captures the specific FITC or Rhodamine Red staining for each protein marker within a tissue (e.g., dorsal horn spinal cord or DRG). Once the optimal level of fluorescent threshold was determined for a particular protein marker, this level was held consistent throughout all of the treatment groups for the image analysis (Fig. 1D). These steps were followed by software conversion of fluorescent wavelength intensity for each fluorophore to a numerical value. Autofluorescence was defined as the emission outside the defined wavelength of interest (e.g., DAPI, 488 ± 10 nm; FITC, 575 ± 5 nm; Rhodamine Red 600 ± 5 nm). These specific autofluorescent and low-level background emission values were subtracted from the image (Fig. 1E and 1F), yielding a numerical value of true fluorescent emission intensity for each fluorophore (Mansfield et al. 2008; Mahad et al. 2009).

Primary antibody staining procedures remained consistent to minimize intensity variations of each fluorophore (FITC or Rhodamine Red) used to detect the different primary antibodies of interest. To ensure that fluorophore binding was not impeded through possible steric hindrance of other proximal fluorophores, sections were labeled for only one cellular marker of interest on a slide.

The user also determined the minimum number of connected pixels on the computer screen for image analysis, counted as a region of interest (ROI) defined in the Nuance software system, which resulted in a software image containing distinctive morphology (i.e., of cellular bodies and processes, pattern of protein expression) that was virtually identical to the morphology observed through the microscope. The number of minimum connected pixels would therefore be set higher for a protein expressed abundantly by a cell (i.e., GFAP) than a protein expressed sparsely, leading to a punctuate pattern (i.e., IL-1$\beta$). These conditions resulted in a region of interest (ROI), and were held consistent for both the ipsilateral and contralateral tissues in every experimental condition and for each antibody stain. The total area of each ROI, as measured by $mm^2$, is calculated and is factored into the overall measurement of fluorescent intensity per second of exposure. The average count of fluorescent emission intensity per second exposure, per $mm^2$ is the analyzed value that we report here. That is, fluorescent intensity average count/sec/$mm^2$, which takes into account the density as well as the intensity of the fluorophore detected. A total of four sections per animal ($N = 3$) were randomly selected and analyzed in this manner. By applying this novel method of data acquisition and analysis, experimenter bias is greatly minimized or even eliminated, yielding greater consistency and objectivity to fluorescent quantification.

### *Data analysis*

Psychometric behavioral analysis was performed as previously described (Milligan et al. 2000) to compute the log stiffness that would have resulted in the 50% paw withdrawal rate. Briefly, thresholds were estimated by fitting a Gaussian integral psychometric function to the observed withdrawal rates for each of the tested von Frey hairs, using a maximum-likelihood fitting method (Treutwein and Strasburger 1999). Estimated thresholds derived from a Gaussian integral function yield a mathematical continuum and thus are appropriate for parametric statistical analyses (Treutwein and Strasburger 1999; Milligan et al. 2000). The computer program PsychoFit may be downloaded from L.O. Harvey's website (http://psych.colorado.edu/~lharvey). All other data analysis was performed using the computer program GraphPad

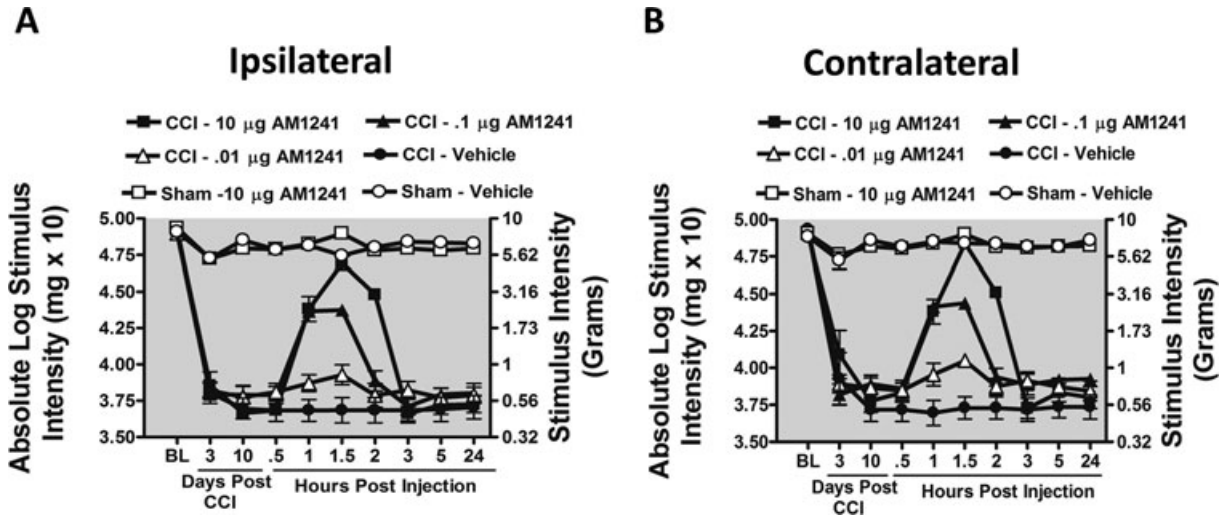


**Figure 2.** Intrathecal (i.t.) AM1241, a cannabinoid 2 receptor agonist reverses CCI-induced allodynia. (**A** and **B**) AM1241 reverses CCI-induced allodynia in a dose-dependent manner. Before surgical manipulation, all AM1241 BL values of experimental groups exhibited similar ipsilateral and contralateral BL thresholds; CCI surgery produced significant bilateral allodynia at Day 3 and 10 following injury compared to sham-treated animals. Responses from AM1241 (10 $\mu$g) maximally reversed CCI-induced allodynia, (black squares), at 1.5 h with allodynia fully returning by 3 h after i.t. administration.

Prism version 4.03 (GraphPad Software Inc., San Diego, CA). For behavioral analysis to assess BL values, a one-way analysis of variance (ANOVA) was applied. To examine the presence of allodynia, a repeated measures ANOVA was used at BL, three and 10 days after CCI, and indicated times note in above section (Behavioral assessment of allodynia). For the initial evaluation of fluorescence fading (Fig. 3A and 3B), the Student's *t* test with a 95% confidence interval was utilized. For all other statistical analysis, a two-way ANOVA with a 95% confidence interval was performed. Statistical significance was determined with *P*-values $< 0.05$. All data are expressed as mean ± SEM. For post hoc analysis, Bonferroni's test was performed.

## Results

### Intrathecal (i.t.) injection of AM1241 reverses CCI-induced allodynia in a dose-dependent manner

Limited evaluation exists for i.t. spinal application of $CB_2R$ agonists to control allodynia produced by CCI, a widely used and well-characterized rodent model of chronic peripheral neuropathy with related pain-like behaviors (Bennett and Xie 1988). We first examined if the putative $CB_2R$ agonist from the aminoalkylindole class, AM1241 (36-fold $CB_2R > CB_1R$) (Yao et al. 2006; Thakur et al. 2009), could reverse ongoing allodynia produced by CCI. Prior to surgical manipulation, all groups exhibited similar bilateral (ipsilateral and contralateral) BL thresholds (ANOVA, $F_{(5,35)} = 1.105$; $P = 0.3764$ and ANOVA, $F_{(5,35)} = 2.632$; $P = 0.5884$, respectively) (Fig. 2A and 2B). Following CCI, clear bilateral allodynia developed by Day 3 and continued chronically through Day 10 compared to sham-operated rats (ANOVA, $F_{(10,56)} = 73.23$; $P < 0.0001$ and ANOVA, $F_{(10,56)} = 71.32$; $P < 0.0001$, respectively). On Day 10, compared to i.t. control injected neuropathic rats, AM1241 produced a dose-dependent reversal of allodynia, with maximal reversal observed at 1.5 h following the highest injected dose (10 $\mu$g). However, allodynia fully returned by 3 h after i.t. AM1241 treatment, with allodynia remaining constant through 24 h. While 0.1 $\mu$g produced attenuated allodynia, 0.01 $\mu$g did not alter allodynia for either the ipsilateral (Fig. 2A) (ANOVA, $F_{(15,84)} = 138.8$; $P < 0.0001$) or contralateral (Fig. 2B) hindpaw responses (ANOVA, $F_{(15,84)} = 131.6$; $P < 0.0001$). Post hoc analysis revealed that 10 $\mu$g AM1241 yielded maximal reversal similar to pretreatment BL values at 1.5 h after injection ($P > 0.05$).

### Spectral analysis versus standard Image J fluorescent analysis

Although previous reports detail an observed increase of IL-1$\beta$ IR within the dorsal horn of the spinal cord after nerve ligation with chromic gut or silk sutures (Hashizume et al. 2000), detecting statistically significant changes in IL-1$\beta$ IR has been problematic. Meanwhile, the use of spectral analysis procedures in other studies has demonstrated increased accuracy and sensitivity for the detection of cell-specific markers (Constantinou et al. 2009; Mahad et al. 2009; Andres et al. 2010). We therefore made direct comparisons between

 

standard fluorescent analysis with Image J software and spectral image analysis software to identify the most sensitive method to quantify immunoreactive proteins of interest. Identical tissue sections for both analysis procedures were used to eliminate potential fluorescent intensity variance between slides. Additionally, FITC-conjugated secondary antibody was examined as well as Rhodamine-conjugated secondary antibody to identify whether intrinsic differences between different fluorophores (red vs. green) could yield false-positive group differences.

IL-1$\beta$ IR was examined with standard FITC fluorescent analysis utilizing NIH Image J software procedures (Fig. 3A). While a trend toward differences was present using Image J software, no statistically significant increase in IL-1$\beta$ IR in either the ipsilateral or contralateral dorsal horn was found between non-neuropathic (Sham-Vehicle) and neuropathic CCI-treated rats (Student's *t* test $P = 0.0620$ and $P = 0.5142$, respectively). We utilized FITC-tagged secondary antibody in these studies because FITC tends to fade at a greater rate than Rhodamine Red, providing a stringent assessment of potential observed differences between experimental groups following a subsequent exposure. We therefore exposed the same tissue sections analyzed in Figure 3A for a second time (Fig. 3B) with double the exposure duration, but with the light sensitivity held consistent. Doubling the exposure time provides a rigorous test to determine whether fading can influence quantitative results. In using Image J, marginal nonsignificant fading of fluorescent intensity (Fig. 3A vs. 3B) (Student's *t* test $P = 0.7418$ and $P = 0.9060$, respectively) was present, and no difference in IL-1$\beta$ IR between nonneuropathic and neuropathic rats was detected (Student's *t* test $P = 0.0648$ and $P = 0.4874$, respectively). In the same context, marginal fading was observed with spectral microscopy exposure between an initial exposure and a subsequent exposure (data not shown).

Given that fluorophore fading was not present upon subsequent exposures, a new set of FITC-stained IL-1$\beta$ tissues from nonneuropathic (Sham-Vehicle) and neuropathic rats (CCI-Vehicle) treatment groups were examined with standard Image J fluorescence analysis followed by spectral analysis. With Image J, we found no significant effect of surgery in either ipsilateral or contralateral dorsal horn (Student *t* test $P = 0.5604$ and $P = 0.6988$, respectively) (Fig. 3C). However, spectral analysis of the identical sections revealed statistically significant differences in ipsilateral IL-1$\beta$ IR due to surgical treatment (Student's *t* test $P = 0.0482$ and $P = 0.0635$, respectively) (Fig. 3D).

We found similar effects following comparison with a new set of slides from L4–L6 lumbar spinal cord tissue sections treated with IL-1$\beta$ primary antibody, but incubated with a secondary antibody conjugated to the Rhodamine Red fluorophore (Fig. 3E and 3F). That is, the quantitative results between FITC or Rhodamine Red fluorescent intensity were similar within each method of image analysis. Specifically, no significant effect from surgical treatment was found utilizing standard Image J Rhodamine Red fluorescence analysis between treatment groups, either ipsilaterally or contralaterally (Student's *t* test $P = 0.2918$ and $P = 0.2023$, respectively) (Fig. 3E), while incorporating spectral analysis methods of the same tissues revealed strong increases in ipsilateral but not contralateral IL-1$\beta$ IR in CCI-treated rats (chronic neuropathy) (Student's *t* test $P = 0.0096$ and $P = 0.1047$, respectively) (Fig. 3F). Representative tissue staining for sham and CCI IL-1$\beta$ are shown, as acquired with standard fluorescent microscopy (Fig. 3G and 3H) and with spectral fluorescent microscopy (Fig. 3I and 3J). Thus, these findings demonstrate that the use of spectral analysis may yield quantitative differences that may have previously gone undetected utilizing standard immunohistochemistry analysis techniques.

## Behavioral verification of i.t. AM1241 for subsequent spinal cord immunohistochemistry

In a separate group of rats, i.t. injection of AM1241 again produced robust bilateral reversal from allodynia (Fig. 4A and 4B), similar to that observed in Figure 2. Prior to CCI, all groups exhibited similar ipsilateral and contralateral BL thresholds (ANOVA, $F_{(3,11)} = 0.9006$; $P = 0.4821$ and ANOVA, $F_{(3,11)} = 0.8916$; $P = 0.4860$, respectively). CCI produced significant bilateral allodynia at Day 3 and continued to Day 10 compared to sham-treated animals (ANOVA, $F_{(1,8)} = 135.8$; $P < 0.0001$ and ANOVA, $F_{(1,8)} = 149.9$; $P = 0.0001$, respectively). Behavioral responses following i.t. AM1241 (10 $\mu$g) produced maximal bilateral reversal of allodynia (ANOVA, $F_{(1,8)} = 150.4$; $P < 0.0001$ and ANOVA, $F_{(1,8)} = 72.36$; $P < 0.0001$, respectively). At peak reversal, animals were sacrificed and spinal tissue was collected to examine bilateral IR for proteins including cytokines p-p38MAPK, glial activation markers, and endocannabinoid degradative enzymes.

## Immunohistochemical analysis of spinal cord dorsal horn

### *IL-10*

While spinal $CB_2R$ activation controls pain-related behaviors and glial activation in neuropathic rats (Zhang et al. 2003; Romero–Sandoval and Eisenach 2007; Racz et al. 2008a,b; Romero–Sandoval et al. 2008b), the underlying spinal immunoregulatory signals remain unclear. One of the most effective anti-inflammatory cytokines characterized to control pathological pain processing to date is IL-10 (Plunkett et al. 2001; Milligan et al. 2005a,b, 2006; Ledeboer et al. 2006; Sloane et al. 2009a,b; Soderquist et al. 2010a,b). Here, we examined changes in IL-10 IR at the time of peak AM1241 efficacy. Bilateral IL-10 IR in the dorsal horn spinal cord

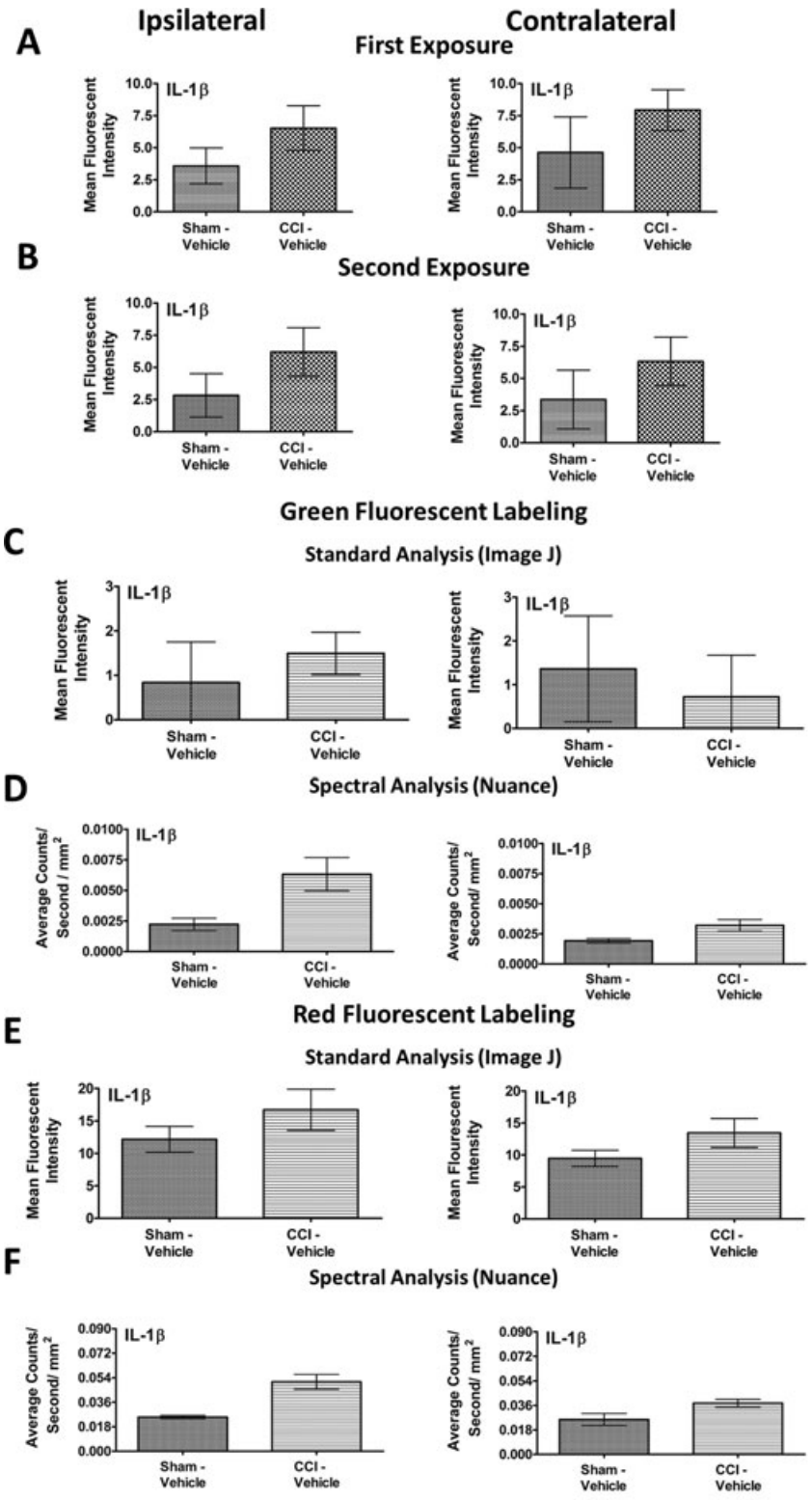


**Figure 3.** Spectral versus standard Image J immunofluorescent intensity quantification comparison. (**A**) Utilizing Image J software for immunofluorescent quantification, no significant IL-1$\beta$ IR differences between CCI-induced neuropathy or nonneuropathic sham-treated rats in either the ipsilateral or contralateral dorsal horn of the spinal cord. IL-1$\beta$ IR was observed by FITC-labeled secondary antibody. (**B**) Following a second exposure for image capture, fluorophore fading was virtually absent thereby lacking potential artificial IR intensity differences between experimental conditions. (**C**) A comparison of sham- and CCI-treated rats with i.t. vehicle using Image J immunofluorescent quantification resulted in no significant fluorescent intensity differences of labeled IL-1$\beta$ IR between groups, in either the ipsilateral or contralateral dorsal horn. (**D**) Utilizing spectral immunofluorescent quantification, significant differences of fluorescent intensity from FITC-labeled IL-1$\beta$ between sham- and CCI-treated rats given i.t. vehicle was observed in the ipsilateral, but not contralateral dorsal horn spinal cord. (**E**) An examination of fluorescent intensity between groups with a flourophore of a different spectral signature, Rhodamine Red (600 nm), using standard Image J immunofluorescent quantification revealed no significant group differences between sham- and CCI-treated rats despite a trend of increased IL-1$\beta$ IR in CCI-treated rats with i.t. vehicle in either the ipsilateral or contralateral dorsal horn. (**F**) Spectral immunofluorescent quantification of Rhodamine Red labeled IL-1$\beta$ yielded significant group differences between nonneuropathic sham rats and CCI-treated rats with vehicle in the ipsilateral dorsal spinal cord. IL-1$\beta$ IR increases were absent in the contralateral dorsal horn. (**G**, **H**) Representative fluorescent images analyzed with Image J at 20$\times$ magnification of IL-1$\beta$ fluorescent labeling (red). (**I**, **J**) Representative spectrally unmixed images at 20$\times$ magnification of IL-1$\beta$ fluorescent labeling (red) with DAPI nuclear stain (blue). In all images, the scale bar is equal to 50 $\mu$m. All sections were 7-$\mu$m thick, and collected 1.5 h after i.t. vehicle administration 10 days after CCI or sham surgery.

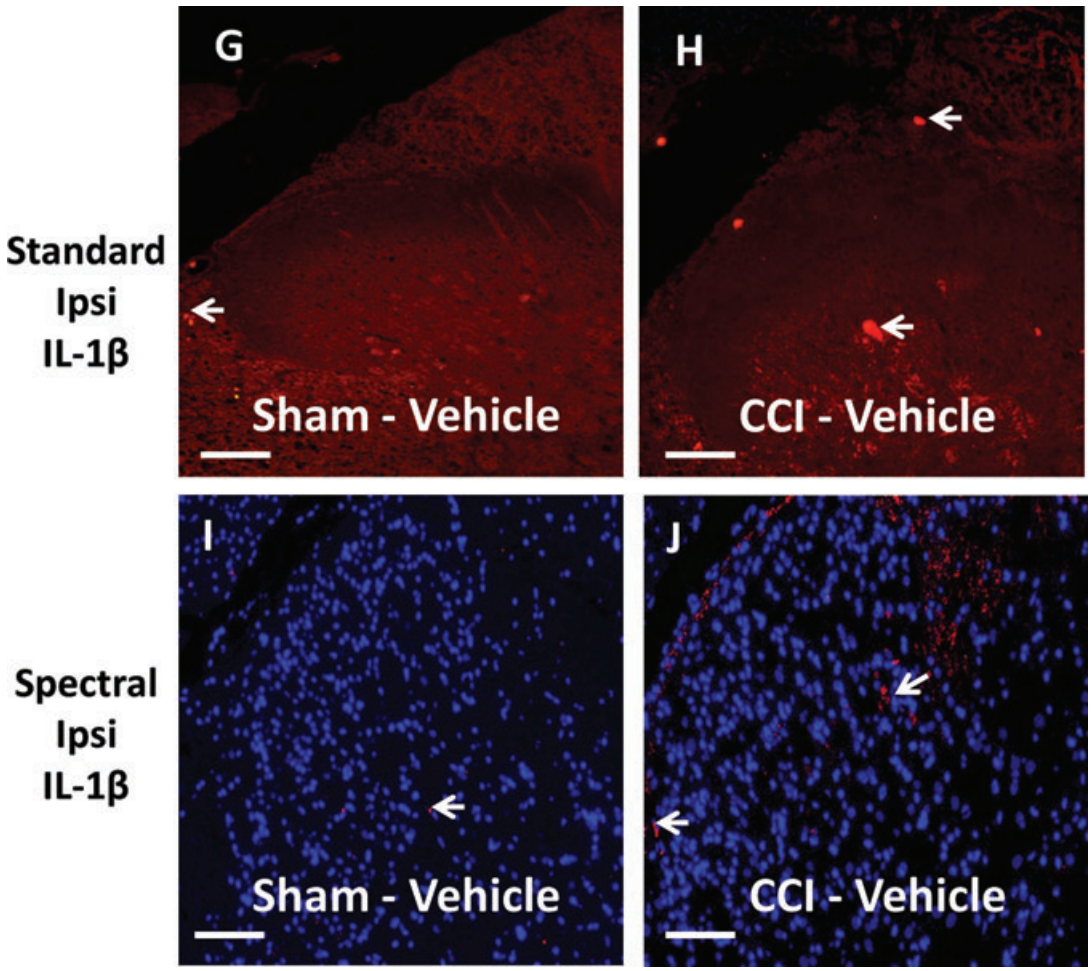


**Figure 3.** Continued

was dramatically decreased in CCI-induced neuropathic rats compared to sham-treated rats (ANOVA, $F_{(1,8)}= 10.09$; $P= 0.0131$ and ANOVA, $F_{(1,8)}= 7.548$; $P= 0.0252$, respectively), (Fig. 4C and 4D). In stark contrast, treatment with AM1241 resulted in basal levels of IL-10 IR, for both the ipsilateral and contralateral dorsal spinal cord (ANOVA, $F_{(1,8)}= 13.19$; $P= 0.0067$ and ANOVA, $F_{(1,8)}= 7.903$; $P= 0.0228$, respectively).

### *IL-1β*

To replicate our results described in Figure 3D and 3F, separate L4–L6 lumbar spinal cord tissue sections were processed and analyzed. Compared to non-neuropathic sham-operated rats given i.t. AM1241 or equivolume vehicle, CCI-induced neuropathy produced a robust unilateral increase in dorsal horn IL-1$\beta$ IR (ANOVA, $F_{(1,8)} = 10.46$; $P = 0.0120$), while, compared to controls, no differences in contralateral IL-1$\beta$ were observed (ANOVA, $F_{(1,8)} = 1.627$; $P = 0.2379$) (Fig. 4E and 4F). Conversely, following AM1241 administration, significantly lower levels of IL-1$\beta$ IR were detected (ANOVA, $F_{(1,8)} = 9.431$; $P = 0.0153$). IL-1$\beta$ IR observed in the contralateral dorsal horn was not substantially elevated when compared to vehicle-injected animals (ANOVA, $F_{(1,8)} = 1.321$; $P = 0.2836$).

### *p38-MAPK and DAPI*

Spinal p-p38MAPK is widely characterized to mediate allodynia through the actions of spinal IL-1$\beta$ (Ji and Suter 2007; Ji et al. 2009). Therefore, p-p38MAPK was examined. Compared to non-neuropathic sham-operated rats given i.t. AM1241 or equivolume vehicle, CCI-induced neuropathy produced a robust p-p38MAPK bilateral IR increase in the spinal cord dorsal horn (ANOVA, $F_{(1,8)}= 223.1$; $P < 0.0001$ and ANOVA, $F_{(1,8)} = 148.0$; $P < 0.0001$, respectively) (Fig. 4G and 4H). In contrast, tissues from rats treated with i.t. AM1241 revealed dramatically lower levels of p-p38MAPK IR that were close to or similar to spinal cord tissues from non-neuropathic

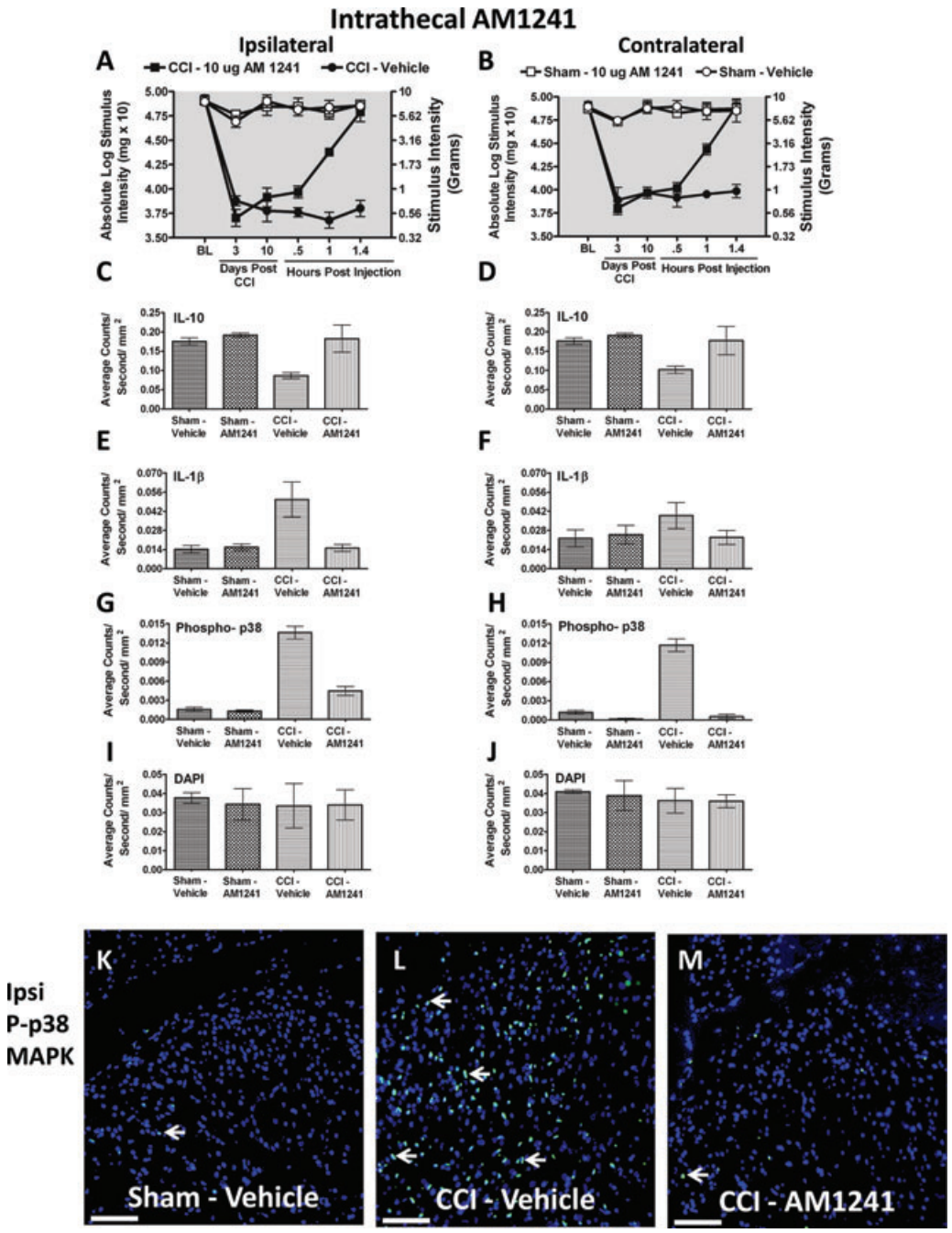


**Figure 4.** Immunofluorescent intensity quantification from 7-$\mu$m thick sections of dorsal horn spinal cord from behaviorally verified rats following i.t. vehicle or AM1241. (**A**, **B**) Prior to CCI, all groups exhibited similar ipsilateral and contralateral BL thresholds. CCI produced significant bilateral allodynia at Day 3 and 10 following injury compared to sham-treated animals. Behavioral responses following AM1241 (10 $\mu$g) produced maximal bilateral reversal of allodynia followed by tissue collection of immunofluorescent intensity quantification. (**C**, **D**) IL-10 expression was bilaterally decreased in CCI-treated rats that received i.t. vehicle compared to control sham-treated rats given either vehicle or AM1241, while IL-10 IR recovered to sham levels in CCI neuropathic rats given i.t. AM1241. (**E**, **F**) Compared to sham controls, IL-1$\beta$ expression was increased ipsilaterally, but not contralaterally in CCI-treated animals given i.t. vehicle of AM1241. However, i.t. AM1241 in CCI-treated rats robustly suppressed increases in IL-1$\beta$ IR. (**G**, **H**) Phospho-p38 expression was bilaterally increased in CCI-induced neuropathic rats treated with i.t vehicle of AM1241. Increased bilateral p-p38MAPK was significantly suppressed in CCI-treated rats given i.t. AM1241. (**I**, **J**) No differences in DAPI nuclear stain fluorescent intensity were observed in either sham control or CCI-treated rats given either i.t. vehicle or AM1241. (**K**, **L**, and **M**) Representative spectrally unmixed images at 20× magnification of p-p38 MAPK fluorescent labeling (green) with DAPI nuclear stain (blue). In all images, the scale bar is equal to 50 $\mu$m.

sham-treated rats (ANOVA, $F_{(1,8)} = 85.82$; $P < 0.0001$ and ANOVA, $F_{(1,8)} = 187.1$; $P < 0.0001$, respectively). Representative fluorescent images are presented corresponding to the image analysis of either sham treated with i.t. vehicle (Fig. 4K), CCI treated with i.t. vehicle (Fig. 4L), or CCI treated with AM1241 (Fig. 4M).

It is possible that overall changes in spinal cord cell numbers could dramatically alter dorsal horn immunofluorescent intensity quantification, as proliferation of microglia (Suter et al. 2009), astrocytes (Tsuda et al. 2011), or leukocyte CNS extravasation (Xu et al. 2007) have been reported. Consequently, cells could simply be constitutively expressing low levels of proteins, thus diminishing interpretation that a protein-specific cellular response has occurred following either CCI and/or i.t. AM1241. However, we observed no change in cell numbers as assessed by quantification of nuclear-specific DAPI fluorescence intensity as a consequence of either CCI procedures (ANOVA, $F_{(1,8)} = 0.1076$; $P = 0.7514$ and ANOVA, $F_{(1,8)} = 0.7780$; $P = 0.4035$, respectively) or i.t. drug injections (ANOVA, $F_{(1,8)} = 0.04328$; $P = 0.8404$ and ANOVA, $F_{(1,8)} = 0.06960$; $P = 0.7986$, respectively) (Fig. 4I and 4J).

## Microglial and astrocyte activation

### *Iba-1 to identify altered microglial responses*

Based on reported evidence that $CB_2$Rs are present on microglia, we examined whether bilateral dorsal spinal microglial responses during CCI-induced allodynia were altered subsequent to i.t. administration of AM1241. To examine microglia in the dorsal horn of the spinal cord, expression of the microglial marker, Iba-1 was examined. Compared to non-neuropathic sham-operated rats given i.t. AM1241 or equivolume vehicle, CCI-induced neuropathy produced a robust bilateral increase in spinal cord dorsal horn Iba-1 IR (ANOVA, $F_{(1,8)} = 212.0$; $P < 0.0001$ and ANOVA, $F_{(1,8)} = 62.28$; $P < 0.0001$, respectively) (Fig. 5A and 5B). Surprisingly, AM1241 did not alter increased levels of spinal dorsal horn Iba-1 IR in behaviorally reversed rats (ipsilateral ANOVA, $F_{(1,8)} = 2.767$; $P = 0.1348$, contralateral ANOVA, $F_{(1,8)} = 0.1346$; $P = 0.7232$) (Fig. 5A and 5B). Representative images taken from the spinal cord dorsal horn following i.t. vehicle injection in sham- and CCI-treated rats are provided (Fig. 5C and 5D).

### *GFAP to identify altered astrocyte responses*

In the superficial dorsal horn, where incoming signals from pain fibers are processed, histological observation reveals that astrocytes make intimate contact with microglia that express $CB_2$Rs (Romero–Sandoval et al. 2008a). Prior reports additionally show that following spinal $CB_2$R activation in neuropathic rats, superficial dorsal horn GFAP IR is significantly reduced (Romero–Sandoval et al. 2009). Therefore, we examined GFAP IR in the dorsal horn following i.t. administration of AM1241. Compared to non-neuropathic control animals, neuropathic rats demonstrated a robust bilateral increase in dorsal horn GFAP IR (ipsilateral ANOVA, $F_{(1,8)} = 15.00$; $P = 0.0047$; contralateral ANOVA, $F_{(1,8)} = 10.45$; $P = 0.0120$) (Fig. 5E and 5F). In stark contrast, lower values of bilateral GFAP IR were observed from tissues of rats treated with i.t. AM1241 (ipsilateral ANOVA, $F_{(1,8)} = 41.38$; $P = 0.0002$; contralateral ANOVA, $F_{(1,8)} = 17.63$; $P = 0.0030$) (Fig. 5E and 5F). Corresponding representative fluorescent images used for analysis are shown; sham-operated rats treated with either i.t. AM1241 or equivolume vehicle (Fig. 3G and 3H), or CCI-treated rats injected with either i.t. AM1241 or equivolume vehicle (Fig. 3I and 3J).

## Monoacylglycerol lipase (MAGL) and fatty acid amide hydrolase (FAAH)

### *MAGL*

Endocannabinoids known to produce anti-allodynic effects are metabolized via enzymatic hydrolysis by fatty acid amide hydrolase (FAAH) and/or MAGL (Basavarajappa 2007). Inhibition of FAAH or MAGL increases the bioavailablity of CNS endocannabinoids with a corresponding attenuation of neuropathic pain rats (Kinsey et al. 2009; Long et al. 2009). Whether FAAH and MAGL IR expression levels are altered in the dorsal horn following i.t. $CB_2$R agonist injections in neuropathic rats, is unknown. Therefore, we examined potential changes in MAGL and FAAH IR in tissue sections from rats given i.t. AM1241. Compared to non-neuropathic control rats, neuropathic rats showed a robust ipsilateral (ANOVA, $F_{(1,8)} = 34.19$; $P = 0.0004$) and contralateral (ANOVA, $F_{(1,8)} = 27.51$; $P = 0.0008$) increase in dorsal horn MAGL IR (Fig. 6A and 6B). In contrast, spinal tissue collected from rats given an i.t. AM1241 injection revealed significantly lower bilateral MAGL IR (ipsilateral ANOVA, $F_{(1,8)} = 8.356$; $P = 0.0202$; contralateral ANOVA, $F_{(1,8)} = 4.146$; $P = 0.0761$, respectively) (Fig. 6A and 6B). Interestingly, no interpretable or meaningful change in FAAH IR between non-neuropathic and neuropathic CCI rats was observed following surgical manipulation (ipsilateral ANOVA, $F_{(1,8)} = 8.072$; $P = 0.0218$; contralateral ANOVA, $F_{(1,8)} = 0.09666$; $P = 0.7638$), or following i.t. AM1241 or vehicle treatment (ANOVA, $F_{(1,8)} = 0.5436$; $P = 0.4820$ and ANOVA, $F_{(1,8)} = 2.174$; $P = 0.1786$, respectively) (Fig. 6C and 6D).

## DRG Immunohistochemical analysis: GFAP, IL-1$\beta$, p-p38MAPK, and IL-10

Immunohistochemical detection of GFAP, IL-1$\beta$, p-p38MAPK, and anti-inflammatory IL-10 in L4–L5 DRG that correspond to the ipsilateral and contralateral spinal cord segments was quantified. Results revealed that compared to non-neuropathic control rats, CCI-induced neuropathic rats

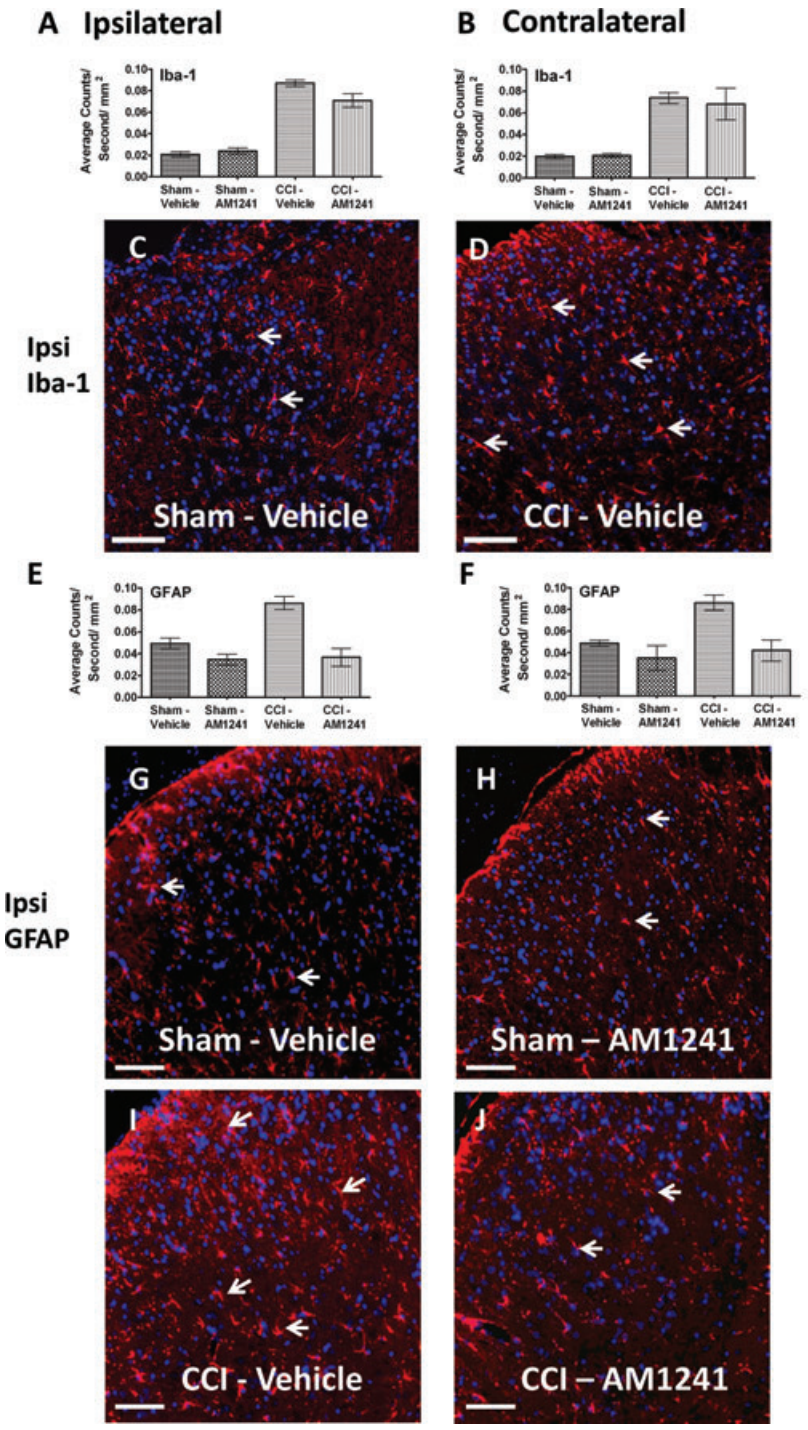


**Figure 5.** Immunofluorescent intensity quantification of the spinal cord dorsal horn reveals differences in astrocyte activation but not microglial activation in neuropathic rats treated with AM1241. (**A**, **B**) Iba-1 expression increased within the ipsilateral and contralateral dorsal horn of the spinal cord following CCI manipulations compared to control sham treatment, irrespective of i.t. vehicle or AM1241. (**C**, **D**) Representative spectrally unmixed images at 20× of Iba-1 fluorescent staining (red) and DAPI nuclear stain (blue). (**E**, **F**) GFAP immunofluorescent intensity in the dorsal horn of the spinal cord was significantly increased in neuropathic rats following CCI given i.t. vehicle, while GFAP IR in neuropathic rats given i.t. AM1241 was greatly attenuated. (**G**, **H**, **I**, and **J**) Representative spectrally unmixed images at 20× magnification of GFAP fluorescent labeling (red) with DAPI nuclear stain (blue). In all images, the scale bar is equal to 50 $\mu$m. All sections were 7 $\mu$m in thickness.

displayed a robust bilateral increase in GFAP IR in DRG (ipsilateral ANOVA, $F_{(1,8)} = 9.133$; $P = 0.0165$; contralateral ANOVA, $F_{(1,8)} = 8.443$; $P = 0.0197$, respectively) (Fig. 7A and 7B). However, i.t. AM1241 injection robustly blocked bilateral increases in GFAP IR (ipsilateral ANOVA, $F_{(1,8)} = 27.19$; $P = 0.0008$; contralateral ANOVA, $F_{(1,8)} = 5.223$; $P = 0.0516$, respectively) (Fig. 7A and 7B). Intriguingly, DRG changes in levels of p-p38MAPK IR occurred in the ipsilateral (ANOVA, $F_{(1,8)} = 6.885$; $P = 0.0305$), but not the contralateral DRG (ANOVA, $F_{(1,8)} = 0.2013$; $P = 0.6656$) to

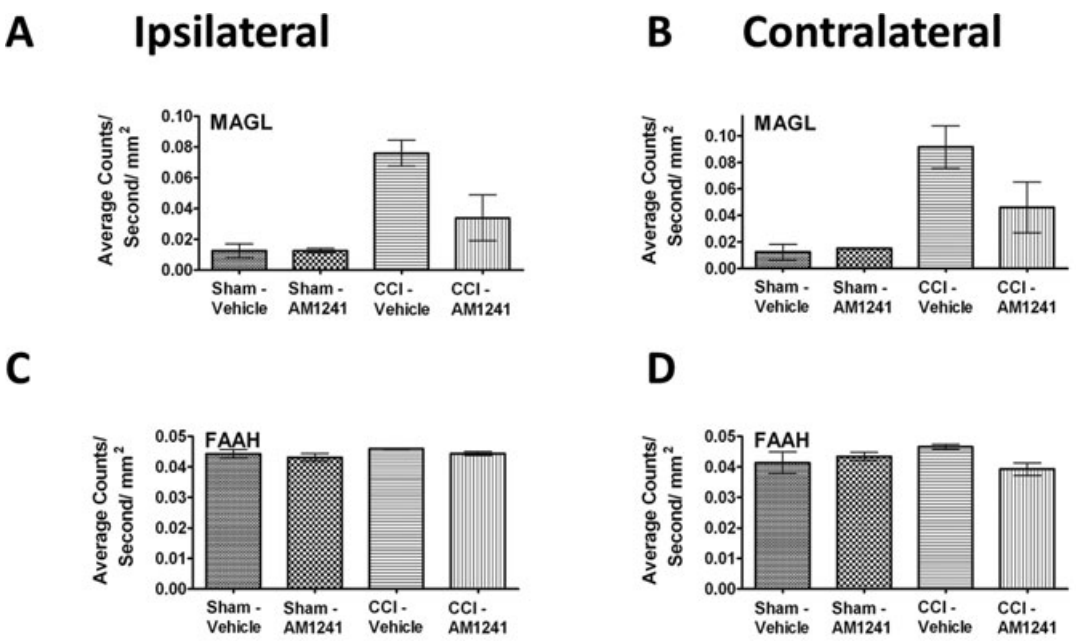


**Figure 6.** Immunofluorescent intensity quantification of the spinal cord dorsal horn reveals that AM1241 reduces the expression of the endocannabinoid degradative enzyme, MAGL but does not alter FAAH. (**A**, **B**) Compared to control rats, MAGL IR expression was increased ipsilaterally, with strong trends contralaterally in CCI-treated neuropathic rats that received i.t vehicle of AM1241, while spinal MAGL IR in CCI-treated rats given i.t. AM1241 was substantially reduced. (**C**, **D**) No changes in FAAH IR expression in ipsilateral and contralateral dorsal horn of either sham- or CCI-neuropathic rats given either i.t. vehicle or AM1241 was observed. All sections were 7 $\mu$m in thickness.

the sciatic nerve damage (Fig. 7C and 7D), and i.t. AM1241 injection revealed ipsilateral p-p38MAPK IR that was similar to controls (ANOVA, $F_{(1,8)} = 15.92$; $P = 0.0040$). No change in p38MAPK IR was detected in the contralateral DRG (ANOVA, $F_{(1,8)} = 2.051$; $P = 0.1900$). This unilateral change was also observed with IL-1$\beta$ IR due to CCI surgery (ipsilateral ANOVA, $F_{(1,8)} = 6.414$; $P = 0.0351$; contralateral ANOVA, $F_{(1,8)} = 0.3111$; $P = 0.5923$), and AM1241 treatment resulted in levels similar to controls (ipsilateral ANOVA, $F_{(1,8)} = 52.03$; $P < 0.0001$; contralateral ANOVA, $F_{(1,8)} = 0.2221$; $P = 0.6500$) (Fig. 7E and 7F). An intriguing unilateral decrease in IL-10 IR was measured in CCI neuropathic rats only (ipsilateral ANOVA, $F_{(1,8)} = 17.42$; $P = 0.0031$; contralateral ANOVA, $F_{(1,8)} = 1.583$; $P = 0.2438$), while an i.t. AM1241 injection resulted in increased IL-10 IR levels that were similar to controls (ipsilateral ANOVA, $F_{(1,8)} = 22.83$; $P = 0.0014$; contralateral ANOVA, $F_{(1,8)} = 1.327$; $P = 0.2826$) (Fig. 7G and 7H). Collectively, these data show that while GFAP-positive satellite cells in bilateral DRG are a target of AM1241, only ipsilateral IL-1$\beta$, p-p38MAPK, and IL-10 IR levels are altered.

## Discussion

In the present study, we examined the efficacy of an i.t. $CB_2R$ agonist, AM1241, on chronic bilateral allodynia produced by unilateral sciatic nerve CCI. We present evidence that AM1241 produced robust bilateral reversal from allodynia in a dose-dependent manner that may act via anti-inflammatory mechanisms. While prior reports show that peripheral administration of AM1241 controls peripheral neuropathy induced by spinal nerve ligation (Ibrahim et al. 2003; Yao et al. 2009), pain from cancer chemotherapeutic agents (Rahn et al. 2007, 2010), and other pathological pain states (Nackley et al. 2004; Beltramo et al. 2006; Rahn et al. 2008; Yao et al. 2009), the current results extend these findings by showing that peri-spinal i.t. AM1241 injection acts to reverse CCI-induced allodynia. Importantly, AM1241 itself did not alter normal basal sensory threshold responses at any dose when administered intrathecally, which is distinct from reports showing an anti-nociceptive action at peripheral nerve terminals following peripheral administration of AM1241 that produced increased BL sensory thresholds (Ibrahim et al. 2006; Khanolkar et al. 2007; Rahn et al. 2010).

In this study, we additionally present evidence for distinct profiles of anti-inflammatory protein expression patterns in the dorsal horn of the spinal cord and DRG. In the dorsal horn of neuropathic rats, bilateral IL-10 IR was significantly lower compared to non-neuropathic rats. While a reduction of peripheral nerve or DRG IL-10 mRNA or protein has been reported (Schafers et al. 2003; Jancalek et al. 2010, 2011), to date,

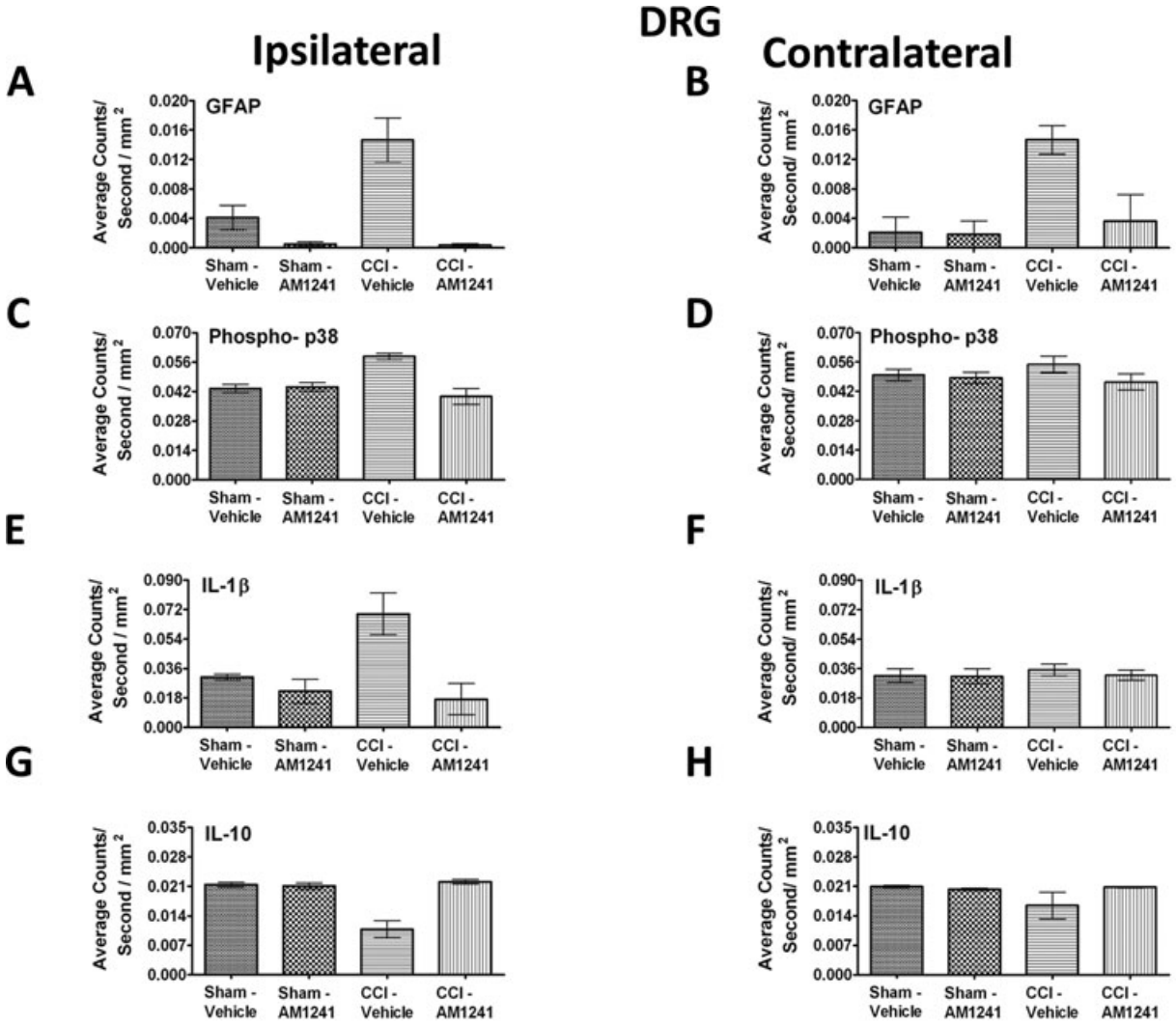


**Figure 7.** Immunofluorescent intensity quantification of 7 $\mu$m in thick sections from the dorsal root ganglion reveals significant differences in satellite cell activation, phosphorylated p38MAPK, IL-1$\beta$, and IL-10 in i.t. AM1241-injected rats. (**A**, **B**) GFAP (satellite cell activation) expression was increased in animals with CCI compared to sham-treated rats, given i.t. vehicle ipsilaterally as well as contralaterally, and robust bilateral suppression of GFAP IR was observed in rats given i.t. AM1241. (**C**, **D**) A small but significant unilateral increase in Phospho-p38 (activated) IR was detected on the side ipsilateral to the CCI treatment with i.t. vehicle, while i.t. AM1241 attenuated increased p-p38MAPK IR in CCI-treated rats. (**E**, **F**) Unilateral IL-1$\beta$ IR was increased in DRG on the side ipsilateral to the CCI manipulation compared to sham-treated controls, while IL-1$\beta$ expression was substantially decreased in CCI-treated rats with i.t. AM1241. (**G**, **H**) Ipsilateral, but not contralateral, IL-10 IR was significantly decreased in CCI-treated neuropathic rats given i.t. vehicle of AM1241 compared to sham controls given either i.t. vehicle or AM1241. However, a robust increase in IL-10 IR in the DRG of CCI-neuropathic rats given i.t. AM1241 was detected.

no prior reports have demonstrated decreased dorsal horn IL-10 IR in adult rats during chronic allodynia from peripheral neuropathy. Additionally, greater bilateral p-p38MAPK, astrocyte GFAP, microglial Iba-1, and MAGL IR levels were measured in neuropathic rats compared to non-neuropathic controls. Further, an increase in unilateral spinal IL-1$\beta$ IR was measured on the side ipsilateral to CCI. However, following an i.t. AM1241 injection, not only was behavioral allodynia reversed, but IL-10, p-p38MAPK, astrocyte GFAP, MAGL, and IL-1$\beta$ IR levels were similar to those observed in non-neuropathic animals. The corresponding L4–L5 DRG immunofluorescent analysis from neuropathic rats revealed similar changes in protein expression patterns, however, bilateral DRG changes were observed only with GFAP IR. These data extend prior reports that AM1241 acts in a general anti-inflammatory manner by identifying specific in vivo spinal

 

and DRG changes of elevated IL-10, with concurrently diminished IL-1$\beta$ and p-p38MAPK IR in the dorsal horn of the spinal cord.

The pattern of bilateral allodynia reported in the current study supports a number of prior reports demonstrating a similar behavioral pattern from CCI (Paulson et al. 2000, 2002; Spataro et al. 2004; Milligan et al. 2005a,b; Xu et al. 2007; Bessiere et al. 2009; Dubovy et al. 2010). Bilateral biochemical changes in the spinal cord and the DRG have been examined that may, in part, characterize underlying contralateral allodynia from CCI. These studies reported decreased $\alpha$2-adrenergic receptor mRNA expression (Leiphart et al. 2003), increased neuronal Fos protein (Ro et al. 2004), increased TNF-$\alpha$ protein (Schafers et al. 2003), and increased IL-6 mRNA expression (Dubovy et al. 2010). Very recent reports have demonstrated increases in unilateral spinal IL-1$\beta$ mRNA expression (Shi et al. 2011), or increased IL-1$\beta$ spinal immunohistochemical detection (Sinicaclo et al. 2011), following unilateral sciatic nerve ligation or transection. Here, we demonstrate the unique findings that an ipsilateral increase in IL-1$\beta$ IR is observed in anatomically intact spinal cord following CCI that produces bilateral allodynia. It is notable that the actions of spinal IL-1$\beta$ are necessary for allodynia produced from CCI (Milligan et al. 2006, 2005a). Together, these data suggest that ipsilateral IL-1$\beta$ is important for initiating changes that ultimately spread to the contralateral spinal cord resulting in contralateral allodynia. Given astrocytes can communicate via gap junctions, it is possible that ipsilateral IL-1$\beta$-to-astrocyte communication leads to the spread of contralateral astrocyte activation via gap junctions inducing signals that result in contralateral allodynia. In support of this hypothesis, a model of localized unilateral sciatic nerve inflammation was demonstrated to critically involve spinal astrocyte gap-junctional communication underlying bilateral allodynia, which was mediated, in part, by spinal IL-1$\beta$ (Spataro et al. 2004). Given the indirect role that ipsilateral IL-1$\beta$ may play in contralateral allodynia, the key biochemical difference between ipsilateral and contralateral spinal cord may be in IL-1$\beta$ expression patterns.

In the current data reported here, we have identified significant increases of IL-1$\beta$ IR in anatomically discrete regions of the spinal cord in CCI-induced neuropathic rats as a consequence of identifying and omitting autofluorescence and low-level background emission intensities from tissue samples. This was achieved by applying relatively straightforward spectral analysis, using the Nuance software, to quantify immunofluorescent levels in anatomically intact spinal cord that eliminates unwanted autofluorescence occurring at nearby wavelengths, which is not discernable using conventional methods of immunofluorescence detection and quantification. Furthermore, we report that i.t. AM1241 resulted in low-level IR for IL-1$\beta$ similar to non-neuropathic control levels that corresponds to anti-allodynia, suggesting that AM1241 inhibits IL-1$\beta$ actions. Indeed, a prior report demonstrated that endogenous IL-1$\beta$ receptor antagonist, IL-1RA, contributes to the anti-inflammatory effects of activated $CB_2$ receptors (Molina–Holgado et al. 2003). Importantly, the discrete IL-1$\beta$ difference between experimental groups detected in the current study was lost when applying standard Image J analysis methods.

The most striking feature of applying spectral analysis to tissue sections with fluorescently tagged protein markers is that autofluorescent emission peaks at nearby wavelengths can be determined from control tissue specimens not stained for the protein marker under examination. The identified autofluorescent wavelengths with corresponding intensity can be subtracted from images derived from tissues that have undergone specific immunohistochemical fluorescence staining procedures. This feature of subtracting "noise" is advantageous when considering that sections between animals within a single experimental group can display variations in peak autofluorescence intensity. Of critical importance is that low-level fluorescence emission within a discrete 10-nm fluorescent wavelength range being analyzed (e.g., FITC 575 nm, $\pm$ 5 nm) can occur in the absence of targeted immunofluorescence protein staining thereby contributing to background "noise." This noise is detected by applying the consistent use of both a fixed contiguous pixel number and fluorescent threshold during image capture. The identified endogenous fluorescent intensity is then omitted from quantification of specific markers in the image. These additional steps ensure experimenter bias is eliminated. A practical consideration is that the spectral analysis software is easily learned and fluorescence-intensity quantification can be conducted in a timely manner. An additional advantage applying immunofluorescent quantification following spectral analysis of intact spinal cord is greater sensitivity to detect specific protein markers compared to other protein quantification procedures that require relatively high amounts of tissue samples (e.g., 100 $\mu$g). These traditional methods often translate into the necessity for greater animal numbers to achieve detectable results.

Proinflammatory factors were examined in this report that extend beyond IL-1$\beta$ in an attempt to provide a broad characterization of the anti-inflammatory effects of $CB_2R$ agonists such as AM1241. The MAPK family consists of three major members that includes p38, which as noted above, contributes to pain sensitization following peripheral nerve injury (Jin et al. 2003; Svensson et al. 2003, 2005a,b; Zhuang et al. 2005, 2007; Ji et al. 2009; Sorkin et al. 2009; Suter et al. 2009) via the actions of spinal IL-1$\beta$ and other proinflammatory cytokines (Liu et al. 2007; Kawasaki et al. 2008). The current data support these prior reports in that increased p-p38MAPK IR is present in the dorsal horn of the spinal cord and DRG in neuropathic rats, and extend AM1241 characterization as an anti-inflammatory $CB_2R$ agonist by

demonstrating that AM1241 robustly suppresses p-p38MAPK IR in pain-reversed rats with peripheral neuropathy.

Here, utilizing microglial and astrocyticmarkers in the spinal cord dorsal horn in neuropathic rats, as assessed by immunofluorescent detection, reveals increased glial responses, in support of prior reports (Schreiber et al. 2008; Obata et al. 2010). Dorsal horn spinal cord astrocyte and microglial responses are recognized to mediate pathological pain in a variety of animal models via p-p38MAPK and IL-1$\beta$ actions (DeLeo et al. 2007; Ji and Suter 2007; Scholz and Woolf 2007). In the CNS, $CB_2R$ mRNA and immunohistochemically identified protein expression is present mostly in spinal microglia (Zhang et al. 2003; Romero–Sandoval and Eisenach 2007; Cabral et al. 2008; Romero–Sandoval et al. 2008a; Racz et al. 2008b), and prior studies reported decreased microglial activation following i.t. administration of $CB_2R$ agonists (Romero–Sandoval and Eisenach 2007; Romero–Sandoval et al. 2009; Toth et al. 2010). Studies examining spinal cords of transgenic $CB_2R$ knockout mice exposed to partial sciatic nerve injury with concurrent neuropathic pain-like behaviors (Racz et al. 2008b) also revealed increased bilateral dorsal horn microglial activation compared to wildtype controls. These results suggest that $CB_2Rs$ play a regulatory role in microglial activation during peripheral neuropathic conditions. However, we report that i.t. AM1241 does not inhibit dorsal spinal microglial activation, as assessed by Iba-1 staining, despite full behavioral reversal of CCI-induced allodynia. Upregulation of Iba-1 is widely known to indicate active microglia (Ohsawa et al. 2000; Ibrahim et al. 2010; Kraft et al. 2011). The differences in the data results may be that the aminoalkylindole, AM1241, acts in a distinctly different manner than other $CB_2R$ agonist compounds, perhaps by inhibiting general spinal proinflammatory processes while leaving microglial function intact. Importantly, increased expression of microglial Iba-1 is indicative of ongoing microglial activity, but cannot distinguish anti-inflammatory versus proinflammatory phenotypes. Thus, it is possible that the increased microglial Iba-1 reported here may be a consequence of increased IL-10 and/or mitogen-activated protein phosphatase production, which are negative regulators to several proinflammatory MAPKs (Romero–Sandoval et al. 2009). This notion is supported by a prior in vitro study that demonstrated $CB_2R$ ligands enhance IL-10 release from immune stimulated macrophages (Correa et al. 2005).

Intriguingly, microglia are an important additional source of the endocannabinoid, 2-arachidonylglycerol (2-AG) (Stella 2009). Endocannabinoids such as anandamide (AEA) and 2-AG are produced and released from neurons and microglia (Walter et al. 2003). Increased endocannabinoid ligand expression and activity in regions such as the spinal cord are characterized to inhibit pain-like behaviors in rats (Martin et al. 1999; Kinsey et al. 2010).

In contrast to persistent microglial activity, i.t. AM1241 reduced bilateral GFAP IR in spinal cord astrocytes and robustly suppressed satellite GFAP IR in the corresponding DRGs. These results support that $CB_2R$ activation reverses chronic bilateral allodynia, in part, by suppressing astrocyte activation. In other studies using immunohistochemical examination of astrocytes and microglia, it is notable that astrocyte end-feet frequently make intimate contact with microglia (Choi et al. 2009; Martin et al. 2010), providing a potential mechanism by which microglia, albeit activated but in an anti-inflammatory manner, can influence astrocyte activation.

The enzyme, MAGL, has been identified on presynaptic axon terminals in brain, suggesting it can terminate 2-AG activity following ligand–receptor internalization in presynaptic neurons (Dinh et al. 2002; Gulyas et al. 2004). The current report supports, but is not limited to, the presynaptic localization of MAGL because immunofluorescent levels were dramatically increased by neuropathy in the superficial dorsal horn where afferent nociceptive fiber terminals communicate to spinal cord pain-processing neurons. These data extend prior reports by showing a strong decrease in spinal MAGL IR following i.t. AM1241 that is concurrent with complete reversal of allodynia. Indeed, MAGL inhibitors decrease allodynia in CCI-induced neuropathic mice (Kinsey et al. 2009), resulting in an increase in 2-AG accumulation that is widely characterized to produce analgesia (Sagar et al. 2009). Microglia also release 2-AG, and MAGL activity has been described in microglia (Muccioli et al. 2007). Together, these data support that decreased MAGL IR may be a result of a generalized decrease in proinflammatory factors following AM1241 treatment.

Surprisingly, an unremarkable unilateral alteration of FAAH was observed following CCI-neuropathy compared to sham controls, and these levels remained unchanged following i.t. AM1241 injection. As such, it is not clear from these data whether FAAH plays an important role in chronic pain produced by CCI-peripheral neuropathy, given these levels remained unchanged during pain reversal. However, only a single biochemical marker was used to ascertain FAAH expression levels. Further, activity of FAAH may not be reflected in its levels of expression. In support of this possibility, reports have demonstrated that blockade of FAAH actions results in anti-allodynia in inflammatory pain models (Booker et al. 2011), or following peripheral nerve transection (Lever et al. 2009), or CCI (Kinsey et al. 2009). Thus, virtually unchanged spinal FAAH IR levels should be cautiously interpreted until further assays verify FAAH expression and activity in models of peripheral neuropathy. Distinct from data in the current report, increased FAAH IR was observed in large diameter DRG neurons following sciatic nerve axotomy or L5 spinal nerve transection (Lever et al. 2009). However, animal models of peripheral axotomy can result in different protein

 

expression profiles in spinal cord and DRG compared to intact damaged axons, as is the case with CCI. These observed differences are frequently reported in different animal models of pathological pain (DeLeo et al. 2007).

DRG satellite cells form a distinct sheath that completely surround sensory neurons, and together with the neuron, create a discrete morphological (Hanani 2005) and a functional unit (Takeda et al. 2009). Satellite DRG glia have gained increasing recognition for altering nociceptive transmission by expressing and responding to several proinflammatory cytokines including IL-1$\beta$ (Takeda et al. 2008, 2009). Indeed, IL-1$\beta$ rapidly activates nociceptive cells in a p38MAPK-dependent manner (Binshtok et al. 2008). The current report supports these reports, as increased expression of p-p38MAPK and IL-1$\beta$, in addition to GFAP, were present in the DRG of neuropathic animals. We demonstrate that ipsilateral DRG IL-10 expression is significantly decreased during CCI-induced chronic neuropathy. Conversely, i.t. treatment with AM1241 resulted in greater p-p38MAPK, IL-1$\beta$, and IL-10 IR levels that are similar to non-neuropathic control basal values. No IL-10, IL-1$\beta$, and p-p38MAPK IR changes in contralateral DRG were observed during CCI-induced chronic allodynia, suggesting these immune signals in contralateral DRG do not play a significant role in CCI-induced contralateral allodynia.

Although AM1241s behavioral effects occur within a relatively short therapeutic half-life ($\sim$1.5 h), these data reveal crucial findings that may support the development of longer lasting, "next generation" $CB_2R$ agonists to produce therapeutic pain control. An advantage of a short therapeutic half-life is the capability to tightly regulate drug loading doses and potential unwanted side effects. Oral formulations easily allow for repeated dosing at discrete intervals. Additionally, a short half-life for i.t. efficacy localized to the spinal cord may be advantageous as it may remain localized to spinal canal, avoiding potential global inhibition of important immune function. Prior reports together with the data presented here support that the actions of AM1241 are highly effective to control pathological pain when delivered either peripherally or by i.t. administration. Additionally, this report supports that pathological pain states, which can include contralateral allodynia ("mirror image" body part) is mediated by significant shifts in ipsilateral and contralateral pro- and anti-inflammatory spinal cord cytokine milieu, as well as shifts in p38MAPK and the endocannabinoid degradative enzyme, MAGL. The implication of these results is that compounds capable of acting on cytokines in the CNS, can therapeutically control clinically relevant centrally and peripherally mediated pathological pain conditions.

## Acknowledgments

The authors would like to thank G. Phillips at the University of New Mexico Cancer Center Shared Microscopy Center for her valuable input and training on the spectral software utilized. This work was supported by NIH grants: NIDA 018156, GM60201. This project was also funded in part by the Dedicated Health Research Funds from the University of New Mexico School of Medicine.

## Conflict of interest

The authors would like to disclose a conflict of interest. A.M. is a consultant for MAK Scientific.

### References

Achstatter, T., R. Moll, A. Anderson, C. Kuhn, S. Pitz, K. Schwechheimer, and W. W. Franke. 1986. Expression of glial filament protein (GFP) in nerve sheaths and non-neural cells re-examined using monoclonal antibodies, with special emphasis on the co-expression of GFP and cytokeratins in epithelial cells of human salivary gland and pleomorphic adenomas. Differentiation 31:206–227.

Andres, C., S. Meyer, O. A. Dina, J. D. Levine, and T. Hucho. 2010. Quantitative automated microscopy (QuAM) elucidates growth factor specific signalling in pain sensitization. Mol. Pain 6:98.

Basavarajappa, B. S. 2007. Critical enzymes involved in endocannabinoid metabolism. Protein Pept. Lett. 14:237–246.

Bellucci, A., A. J. Westwood, E. Ingram, F. Casamenti, M. Goedert, and M. G. Spillantini. 2004. Induction of inflammatory mediators and microglial activation in mice transgenic for mutant human P301S tau protein. Am. J. Pathol. 165:1643–1652.

Beltramo, M., N. Bernardini, R. Bertorelli, M. Campanella, E. Nicolussi, S. Fredduzzi, and A. Reggiani. 2006. $CB_2$ receptor-mediated antihyperalgesia: possible direct involvement of neural mechanisms. Eur. J. Neurosci. 23:1530–1538.

Bennett, G. J., and K. Y. Xie. 1988. A peripheral mononeuropathy in rat that produces disorders of pain sensation like those seen in man. Pain 33:87–107.

Bessiere, B., E. Laboureyras, J. Chateauraynaud, J. P. Laulin, and G. Simonnet. 2009. A single nitrous oxide (N2O) exposure leads to persistent alleviation of neuropathic pain in rats. J. Pain 11:13–23.

Binshtok, A. M., H. Wang, K. Zimmermann, F. Amaya, D. Vardeh, L. Shi, G. J. Brenner, R. R. Ji, B. P. Bean, C. J. Woolf, et al. 2008. Nociceptors are interleukin-1beta sensors. J. Neurosci. 28:14062–14073.

Booker, L., S. G. Kinsey, R. A. Abdullah, J. L. Blackman, J. Z. Long, C. Ezzili, D. L. Boger, B. F. Cravatt, and A. H. Lichtman. 2011. The FAAH inhibitor PF-3845 acts in the nervous system to reverse lipopolysaccharide-induced tactile allodynia in mice. Br. J. Pharmacol. (In press).

Boyle, D. L., T. L. Jones, D. Hammaker, C. I. Svensson, S. Rosengren, S. Albani, L. Sorkin, and G. S. Firestein. 2006.

 

Regulation of peripheral inflammation by spinal p38 MAP kinase in rats. PLoS Med. 3:e338.

Cabral, G. A., and F. Marciano-Cabral. 2005. Cannabinoid receptors in microglia of the central nervous system: immune functional relevance. J. Leukoc. Biol. 78:1192–1197.

Cabral, G. A., E. S. Raborn, L. Griffin, J. Dennis, and F. Marciano-Cabral. 2008. CB2 receptors in the brain: role in central immune function. Br. J. Pharmacol. 153:240–251.

Chaplan, S. R., F. W. Bach, J. W. Pogrel, J. M. Chung, and T. L. Yaksh. 1994. Quantitative assessment of tactile allodynia in the rat paw. J. Neurosci. Meth. 53:55–63.

Choi, J., D. R. Nordli Jr., T. D. Alden, A. DiPatri Jr., L. Laux, K. Kelley, J. Rosenow, S. U. Schuele, V. Rajaram, and S. Koh. 2009. Cellular injury and neuroinflammation in children with chronic intractable epilepsy. J. Neuroinflammation 6:38.

Constantinou, P., R. S. Dacosta, and B. C. Wilson. 2009. Extending immunofluorescence detection limits in whole paraffin-embedded formalin fixed tissues using hyperspectral confocal fluorescence imaging. J. Microsc. 234:137–146.

Correa, F., L. Mestre, F. Docagne, and C. Guaza. 2005. Activation of cannabinoid CB2 receptor negatively regulates IL-12p40 production in murine macrophages: role of IL-10 and ERK1/2 kinase signaling. Br. J. Pharmacol. 145:441–448.

De Leo, J. A., V. L. Tawfik, and M. L. LaCroix-Fralish. 2006. The tetrapartite synapse: path to CNS sensitization and chronic pain. Pain 122:17–21.

DeLeo, J. A., L. S. Sorkin, and L. R. Watkins, eds. 2007. Immune and glial regulation of pain. IASP Press, Seattle.

Dinh, T. P., T. F. Freund, and D. Piomelli. 2002. A role for monoglyceride lipase in 2-arachidonoylglycerol inactivation. Chem. Phys. Lipids 121:149–158.

Dubovy, P., I. Klusakova, I. Svizenska, and V. Brazda. 2010. Satellite glial cells express IL-6 and corresponding signal-transducing receptors in the dorsal root ganglia of rat neuropathic pain model. Neuron Glia Biol. 6:73–83.

Ehrhart J., D. Obregon, T. Mori, H. Hou, N. Sun, Y. Bai, T. Klein, F. Fernandez, J. Tan, and R. D. Shytle. 2005. Stimulation of cannabinoid receptor 2 (CB2) suppresses microglial activation. J Neuroinflammation 2:1–29.

Fukudome, Y., T. Tabata, T. Miyoshi, S. Haruki, K. Araishi, S. Sawada, and M. Kano. 2003. Insulin-like growth factor-I as a promoting factor for cerebellar Purkinje cell development. Eur. J. Neurosci. 17:2006–2016.

Gulyas, A. I., B. F. Cravatt, M. H. Bracey, T. P. Dinh, D. Piomelli, F. Boscia, and T. F. Freund. 2004. Segregation of two endocannabinoid-hydrolyzing enzymes into pre- and postsynaptic compartments in the rat hippocampus, cerebellum and amygdala. Eur. J. Neurosci. 20:441–458.

Hanani, M. 2005. Satellite glial cells in sensory ganglia: from form to function. Brain Res. Brain Res. Rev. 48:457–476.

Hashizume, H., J. A. DeLeo, R. W. Colburn, and J. N. Weinstein. 2000. Spinal glial activation and cytokine expression after lumbar root injury in the rat. Spine 25:1206–1217.

Holguin, A., K. A. O'Connor, J. Biedenkapp, J. Campisi, J. Wieseler-Frank, E. D. Milligan, M. K. Hansen, L. Spataro, E. Maksimova, C. Bracmann, et al. 2004. HIV-1 gp120 stimulates proinflammatory cytokine-mediated pain facilitation via activation of nitric oxide synthase-I (nNOS). Pain 110:517–530.

Hor, S., H. Pirzer, L. Dumoutier, F. Bauer, S. Wittmann, H. Sticht, J. C. Renauld, R. de Waal Malefyt, and H. Fickenscher. 2004. The T-cell lymphokine interleukin-26 targets epithelial cells through the interleukin-20 receptor 1 and interleukin-10 receptor 2 chains. J. Biol. Chem. 279:33343–33351.

Hsieh, G. C., M. Pai, P. Chandran, B. A. Hooker, C. Z. Zhu, A. K. Salyers, E. J. Wensink, C. Zhan, W. A. Carroll, M. J. Dart, et al. 2011. Central and peripheral sites of action for CB receptor mediated analgesic activity in chronic inflammatory and neuropathic pain models in rats. Br. J. Pharmacol. 162:428–440.

Ibrahim, A. S., M. M. El-Shishtawy, A. Pena Jr., and G. I. Liou. 2010. Genistein attenuates retinal inflammation associated with diabetes by targeting of microglial activation. Mol. Vis. 16:2033–2042.

Ibrahim, M. M., H. Deng, A. Zvonok, D. A. Cockayne, J. Kwan, H. P. Mata, T. W. Vanderah, J. Lai, F. Porreca, A. Makriyannis, et al. 2003. Activation of CB2 cannabinoid receptors by AM1241 inhibits experimental neuropathic pain: pain inhibition by receptors not present in the CNS. Proc. Natl. Acad. Sci. U.S.A. 100:10529–10533.

Ibrahim, M. M., M. L. Rude, N. J. Stagg, H. P. Mata, J. Lai, T. W. Vanderah, F. Porreca, N. E. Buckley, A. Makriyannis, and T. P. Malan Jr. 2006. CB2 cannabinoid receptor mediation of antinociception. Pain 122:36–42.

Imai, Y., I. Ibata, D. Ito, K. Ohsawa, and S. Kohsaka. 1996. A novel gene iba1 in the major histocompatibility complex class III region encoding an EF hand protein expressed in a monocytic lineage. Biochem. Biophys. Res. Commun. 224:855–862.

Jancalek, R., P. Dubovy, I. Svizenska, and I. Klusakova. 2010. Bilateral changes of TNF-alpha and IL-10 protein in the lumbar and cervical dorsal root ganglia following a unilateral chronic constriction injury of the sciatic nerve. J. Neuroinflammation 7:11.

Jancalek, R., I. Svizenska, I. Klusakova, and P. Dubovy. 2011. Bilateral changes of IL-10 protein in lumbar and cervical dorsal root ganglia following proximal and distal chronic constriction injury of peripheral nerve. Neurosci. Lett. 501:86–91.

Ji, R. R., and M. R. Suter. 2007. p38 MAPK, microglial signaling, and neuropathic pain. Mol. Pain 3:33.

Ji, R. R., R. W. Gereaut, M. Malcangio, and G. R. Strichartz. 2009. MAP kinase and pain. Brain Res. Rev. 60:135–148.

Jin, S. X., Z. Y. Zhuang, C. J. Woolf, and R. R. Ji. 2003. p38 mitogen-activated protein kinase is activated after a spinal nerve ligation in spinal cord microglia and dorsal root ganglion neurons and contributes to the generation of neuropathic pain. J. Neurosci. 23:4017–4022.

 

Kawasaki, Y., Z. Z. Xu, X. Wang, J. Y. Park, Z. Y. Zhuang, P. H. Tan, Y. J. Gao, K. Roy, G. Corfas, E. H. Lo, et al. 2008. Distinct roles of matrix metalloproteases in the early- and late-phase development of neuropathic pain. Nat. Med. 14:331–336.

Khanolkar, A. D., D. Lu, M. Ibrahim, R. I. Duclos Jr., G. A. Thakur, T. P. Malan Jr., F. Porreca, V. Veerappan, X. Tian, C. George, et al. 2007. Cannabilactones: a novel class of CB2 selective agonists with peripheral analgesic activity. J. Med. Chem. 50:6493–6500.

Kinsey, S. G., J. Z. Long, S. T. O'Neal, R. A. Abdullah, J. L. Poklis, D. L. Boger, B. F. Cravatt, and A. H. Lichtman. 2009. Blockade of endocannabinoid-degrading enzymes attenuates neuropathic pain. J. Pharmacol. Exp. Ther. 330:902–910.

Kinsey, S. G., J. Z. Long, B. F. Cravatt, and A. H. Lichtman. 2010. Fatty acid amide hydrolase and monoacylglycerol lipase inhibitors produce anti-allodynic effects in mice through distinct cannabinoid receptor mechanisms. J. Pain 11:1420–1428.

Kraft, A. D., L. S. Kaltenbach, D. C. Lo, and G. J. Harry. 2011. Activated microglia proliferate at neurites of mutant huntingtin-expressing neurons. Neurobiol. Aging 3:621.e17–621.e33.

Ledeboer, A., E. M. Sloane, E. D. Milligan, S. J. Langer, S. F. Maier, K. W. Johnson, L. A. Leinwand, R. A. Chavez, and L. R. Watkins. 2006. Paclitaxel-induced mechanical allodynia in rats is inhibited by spinal delivery of plasmid DNA encoding interleukin-10. Pp. 187–194 *in* H. Flor, E. Kalso, and J. O. Dostrovsky, eds. Proceedings of the 11th World Congress on Pain. International Association for the Study of Pain, Sydney, Australia.

Leiphart, J. W., C. V. Dills, and R. M. Levy. 2003. Decreased spinal alpha2a- and alpha2c-adrenergic receptor subtype mRNA in a rat model of neuropathic pain. Neurosci. Lett. 349:5–8.

Lever, I. J., M. Robinson, M. Cibelli, C. Paule, P. Santha, L. Yee, S. P. Hunt, B. F. Cravatt, M. R. Elphick, I. Nagy, et al. 2009. Localization of the endocannabinoid-degrading enzyme fatty acid amide hydrolase in rat dorsal root ganglion cells and its regulation after peripheral nerve injury. J. Neurosci. 29:3766–3780.

Liu, Y. L., L. J. Zhou, N. W. Hu, J. T. Xu, C. Y. Wu, T. Zhang, Y. Y. Li, and X. G. Liu. 2007. Tumor necrosis factor-alpha induces long-term potentiation of C-fiber evoked field potentials in spinal dorsal horn in rats with nerve injury: the role of NF-kappa B, JNK and p38 MAPK. Neuropharmacology 52:708–715.

Long, J. Z., D. K. Nomura, R. E. Vann, M. Walentiny, L. Booker, X. Jin, J. J. Burston, L. J. Sim-Selley, A. H. Lichtman, J. L. Wiley, et al. 2009. Dual blockade of FAAH and MAGL identifies behavioral processes regulated by endocannabinoid crosstalk in vivo. Proc. Natl. Acad. Sci. U.S.A. 106:20270–20275.

Loram, L. C., J. A. Harrison, E. M. Sloane, M. R. Hutchinson, P. Sholar, F. R. Taylor, D. Berkelhammer, B. D. Coats, S. Poole, E. D. Milligan, et al. 2009. Enduring reversal of neuropathic pain by a single intrathecal injection of adenosine 2A receptor agonists: a novel therapy for neuropathic pain. J. Neurosci. 44:14015–14025.

Mahad, D. J., I. Ziabreva, G. Campbell, F. Laulund, J. L. Murphy, A. K. Reeve, L. Greaves, K. J. Smith, and D. M. Turnbull. 2009. Detection of cytochrome c oxidase activity and mitochondrial proteins in single cells. J. Neurosci. Methods 184: 310–319.

Mansfield, J. R., C. Hoyt, and R. M. Levenson. 2008. Visualization of microscopy-based spectral imaging data from multi-label tissue sections. Curr. Protoc. Mol. Biol., Chapter 14, Unit 14–19.

Marquez, L., J. Suarez, M. Iglesias, F. J. Bermudez-Silva, F. Rodriguez de Fonseca, and M. Andreu. 2009. Ulcerative colitis induces changes on the expression of the endocannabinoid system in the human colonic tissue. PLoS One 4:e6893.

Martin, A., R. Boisgard, B. Theze, N. Van Camp, B. Kuhnast, A. Damont, M. Kassiou, F. Dolle, and B. Tavitian. 2010. Evaluation of the PBR/TSPO radioligand [(18)F]DPA-714 in a rat model of focal cerebral ischemia. J. Cereb. Blood Flow Metab. 30:230–241.

Martin, W. J., C. M. Loo, and A. I. Basbaum. 1999. Spinal cannabinoids are anti-allodynic in rats with persistent inflammation. Pain 82:199–205.

Milligan, E. D., and L. R. Watkins. 2009. Pathological and protective roles of glia in chronic pain. Nat. Rev. Neurosci. 10:23–36.

Milligan, E. D., K. K. Mehmert, J. L. Hinde, L. O. J. Harvey, D. Martin, K. J. Tracey, S. F. Maier, and L. R. Watkins. 2000. Thermal hyperalgesia and mechanical allodynia produced by intrathecal administration of the Human Immunodeficiency Virus-1 (HIV-1) envelope glycoprotein, gp120. Brain Res. 861:105–116.

Milligan, E. D., S. J. Langer, E. M. Sloane, L. He, J. Wieseler-Frank, K. A. O'Connor, D. Martin, J. R. Forsayeth, S. F. Maier, K. Johnson, et al. 2005a. Controlling pathological pain by adenovirally driven spinal production of the anti-inflammatory cytokine, Interleukin-10. Eur. J. Neurosci. 21:2136–2148.

Milligan, E. D., E. M. Sloane, S. J. Langer, P. E. Cruz, M. Chacur, L. Spataro, Wieseler-J. Frank, S. E. Hammack, S. F. Maier, T. R. Flotte, et al. 2005b. Controlling neuropathic pain by adeno-associated virus driven production of the anti-inflammatory cytokine, interleukin-10. Mol. Pain 1:9–22.

Milligan, E. D., E. M. Sloane, S. J. Langer, T. R. Hughes, B. M. Jekich, M. G. Frank, J. H. Mahoney, L. H. Levkoff, S. F. Maier, P. E. Cruz, et al. 2006. Repeated intrathecal injections of plasmid DNA encoding interleukin-10 produce prolonged reversal of neuropathic pain. Pain 126:294–308.

Milligan, E. D., R. G. Soderquist, S. M. Malone, J. H. Mahoney, T. S. Hughes, S. J. Langer, E. M. Sloane, S. F. Maier, L. A. Leinwand, L. R. Watkins, et al. 2007. Intrathecal polymer-based interleukin-10 gene delivery for neuropathic pain. Neuron Glia Biol. 2:1–16.

Molina-Holgado, F., E. Pinteaux, J. D. Moore, Molina-E. Holgado, C. Guaza, R. M. Gibson, and N. J. Rothwell. 2003. Endogenous interleukin-1 receptor antagonist mediates anti-inflammatory and neuroprotective actions of cannabinoids in neurons and glia. J. Neurosci. 23:6470–6474.

Muccioli, G. G., C. Xu, E. Odah, E. Cudaback, J. A. Cisneros, D. M. Lambert, M. L. Lopez Rodriguez, S. Bajjalieh, and N. Stella. 2007. Identification of a novel endocannabinoid-hydrolyzing enzyme expressed by microglial cells. J. Neurosci. 27:2883–2889.

Nackley, A. G., A. M. Zvonok, A. Makriyannis, and A. G. Hohmann. 2004. Activation of cannabinoid CB2 receptors suppresses C-fiber responses and windup in spinal wide dynamic range neurons in the absence and presence of inflammation. J. Neurophysiol. 92:3562–3574.

Nunez, E., C. Benito, R. M. Tolon, C. J. Hillard, W. S. Griffin, and J. Romero. 2008. Glial expression of cannabinoid CB(2) receptors and fatty acid amide hydrolase are beta amyloid-linked events in Down's syndrome. Neuroscience 151:104–110.

Obata, H., S. Sakurazawa, M. Kimura, and S. Saito. 2010. Activation of astrocytes in the spinal cord contributes to the development of bilateral allodynia after peripheral nerve injury in rats. Brain Res. 1363:72–80.

Ohsawa, K., Y. Imai, H. Kanazawa, Y. Sasaki, and S. Kohsaka. 2000. Involvement of Iba1 in membrane ruffling and phagocytosis of macrophages/microglia. J. Cell Sci. 113(Pt 17):3073–3084.

Paulson, P. E., T. J. Morrow, and K. L. Casey 2000. Bilateral behavioral and regional cerebral blood flow changes during painful peripheral mononeuropathy in the rat. Pain 84:233–245.

Paulson, P. E., K. L. Casey, and T. J. Morrow. 2002. Long-term changes in behavior and regional cerebral blood flow associated with painful peripheral monotherapy in the rat. Pain 95:31–40.

Pekny, M., and M. Pekna. 2004. Astrocyte intermediate filaments in CNS pathologies and regeneration. J. Pathol. 204:428–437.

Plunkett, J. A., C.-G. Yu, J.m. Easton, J. R. Bethea, and R. P. Yezierski. 2001. Effects of interleukin-10 (IL-10) on pain behavior and gene expression following excitotoxic spinal cord injury in the rat. Exp. Neurol. 168:144–154.

Racz, I., X. Nadal, J. Alferink, J. E. Banos, J. Rehnelt, M. Martin, B. Pintado, A. Gutierrez-Adan, E. Sanguino, N. Bellora, et al. 2008a. Interferon-gamma is a critical modulator of CB(2) cannabinoid receptor signaling during neuropathic pain. J. Neurosci. 28:12136–12145.

Racz, I., X. Nadal, J. Alferink, J. E. Banos, J. Rehnelt, M. Martin, B. Pintado, A. Gutierrez-Adan, E. Sanguino, J. Manzanares, et al. 2008b. Crucial role of CB(2) cannabinoid receptor in the regulation of central immune responses during neuropathic pain. J. Neurosci. 28:12125–12135.

Rahn, E. J., A. Makriyannis, and A. G. Hohmann. 2007. Activation of cannabinoid CB1 and CB2 receptors suppresses neuropathic nociception evoked by the chemotherapeutic agent vincristine in rats. Br. J. Pharmacol. 152:765–777.

Rahn, E. J., A. M. Zvonok, G. A. Thakur, A. D. Khanolkar, A. Makriyannis, and A. G. Hohmann. 2008. Selective activation of cannabinoid CB2 receptors suppresses neuropathic nociception induced by treatment with the chemotherapeutic agent paclitaxel in rats. J. Pharmacol. Exp. Ther. 327:584–591.

Rahn, E. J., A. M. Zvonok, A. Makriyannis, and A. G. Hohmann. 2010. Antinociceptive effects of racemic AM1241 and its chirally synthesized enantiomers: lack of dependence upon opioid receptor activation. AAPS J. 12:147–157.

Reed, J. R., R. P. Leon, M. K. Hall, and K. L. Schwertfeger. 2009. Interleukin-1beta and fibroblast growth factor receptor 1 cooperate to induce cyclooxygenase-2 during early mammary tumourigenesis. Breast Cancer Res. 11:R21.

Ro, L. S., H. Y. Li, K. F. Huang, and S. T. Chen. 2004. Territorial and extra-territorial distribution of Fos protein in the lumbar spinal dorsal horn neurons in rats with chronic constriction nerve injuries. Brain Res. 1004:177–187.

Romero-Sandoval, A., and J. C. Eisenach. 2007. Spinal cannabinoid receptor type 2 activation reduces hypersensitivity and spinal cord glial activation after paw incision. Anesthesiology 106:787–794.

Romero-Sandoval, A., N. Nutile-McMenemy, and J. A. DeLeo. 2008a. Spinal microglial and perivascular cell cannabinoid receptor type 2 activation reduces behavioral hypersensitivity without tolerance after peripheral nerve injury. Anesthesiology 108:722–734.

Romero-Sandoval, E. A., R. J. Horvath, and J. A. Deleo. 2008b. Neuroimmune interactions and pain: focus on glial-modulating targets. Curr. Opin. Investig. Drugs 9:726–734.

Romero-Sandoval, E. A., R. Horvath, R. P. Landry, and J. A. DeLeo. 2009. Cannabinoid receptor type 2 activation induces a microglial anti-inflammatory phenotype and reduces migration via MKP induction and ERK dephosphorylation. Mol. Pain 5:25.

Sagar, D. R., A. G. Gaw, B. N. Okine, S. G. Woodhams, A. Wong, D. A. Kendall, and V. Chapman. 2009. Dynamic regulation of the endocannabinoid system: implications for analgesia. Mol. Pain 5:59.

Schafers, M., C. I. Svensson, C. Sommer, and L. S. Sorkin. 2003. Tumor necrosis factor-alpha induces mechanical allodynia after spinal nerve ligation by activation of p38 MAPK in primary sensory neurons. J. Neurosci. 23:2517–2521.

Scholz, J., and C. J. Woolf. 2007. The neuropathic pain triad: neurons, immune cells, and glia. Nat. Neurosci. 10:1361–1368.

Schreiber, K. L., A. J. Beitz, and G. L. Wilcox. 2008. Activation of spinal microglia in a murine model of peripheral inflammatory induced, long-lasting contralateral allodynia. Neurosci. Lett. 440:63–67.

Shi, X. Q., T. K. Y. Lim, S. Lee, Y. Q. Zhao, and J. Zhang. 2011. Statins alleviate experimental nerve injury-induced neuropathic pain. Pain 152:1033–1043.

 

Siniscalco, D., C. Giordano, U. Galderisi, L. Luongo, V. de Novellis, F. Rossi, and S. Maione. 2011. Long-lasting effects of human mesenchymal stem cell systemic administration on pain-like behaviors, cellular, and biomolecular modifications in neuropathic mice. Front. Integr. Neurosci. 5:1–10.

Sloane, E. M., S. J. Langer, B. M. Jekich, J. H. Mahoney, T. S. Hughes, W. Seibert, K. Johnson, R. A. Chavez, L. R. Watkins, L. A. Leinwand, et al. 2009a. Immunological priming potentiates non-viral anti-inflammatory gene therapy treatment of neuropathic pain. Gene Ther. 16:1210–1222.

Sloane, E. M., R. G. Soderquist, S. F. Maier, M. J. Mahoney, L. R. Watkins, and E. D. Milligan. 2009b. Long-term control of neuropathic pain in a non-viral gene therapy paradigm. Gene Ther. 16:470–475.

Soderquist, R. G., E. D. Milligan, J. A. Harrison, R. Chavez, K. Johnson, L. R. Watkins, and M. J. Mahoney. 2010a. PEGylation of interleukin-10 for the mitigation of enhanced pain states. J. Biomed. Mater. Res. A 3:1169–1179.

Soderquist, R. G., E. M. Sloane, L. C. Loram, J. A. Harrison, E. C. Dengler, S. M. Johnson, L. D. Amer, C. S. Young, M. T. Lewis, S. Poole, et al. 2010b. Release of plasmid DNA-encoding IL-10 from PLGA microparticles facilitates long-term reversal of neuropathic pain following a single intrathecal administration. Pharm. Res. 27:841–854.

Sorkin, L., C. I. Svensson, T. L. Jones-Cordero, M. P. Hefferan, and W. M. Campana. 2009. Spinal p38 mitogen-activated protein kinase mediates allodynia induced by first-degree burn in the rat. J. Neurosci. Res. 87:948–955.

Spataro, L. E., E. M. Sloane, E. D. Milligan, J. Wieseler-Frank, D. Schoeniger, B. M. Jekich, R. M. Barrientos, S. F. Maier, and L. R. Watkins. 2004. Spinal gap junctions: potential involvement in pain facilitation. J. Pain 5:392–405.

Starowicz, K. M., L. Cristino, I. Matias, R. Capasso, A. Racioppi, A. A. Izzo, and V. Di Marzo. 2008. Endocannabinoid dysregulation in the pancreas and adipose tissue of mice fed with a high-fat diet. Obesity (Silver Spring) 16:553–565.

Stella, N. 2009. Endocannabinoid signaling in microglial cells. Neuropharmacology 56(Suppl 1):244–253.

Suter, M. R., T. Berta, Y. J. Gao, I. Decosterd, and R. R. Ji. 2009. Large A-fiber activity is required for microglial proliferation and p38 MAPK activation in the spinal cord: different effects of resiniferatoxin and bupivacaine on spinal microglial changes after spared nerve injury. Mol. Pain 5:53.

Svensson, C. I., M. Marsala, A. Westerlund, N. A. Calcutt, W. M. Campana, J. D. Freshwater, R. Catalano, Y. Feng, A. A. Protter, B. Scott, et al. 2003. Activation of p38 MAP Kinase in spinal microglia is a critical link in inflammation induced spinal pain processing. J. Neurochem. 6:1534–1544.

Svensson, C. I., B. Fitzsimmons, S. Azizi, H. C. Powell, X. Y. Hua, and T. L. Yaksh. 2005a. Spinal p38beta isoform mediates tissue injury-induced hyperalgesia and spinal sensitization. J. Neurochem. 92:1508–1520.

Svensson, C. I., M. Schafers, T. L. Jones, H. Powell, and L. S. Sorkin. 2005b. Spinal blockade of TNF blocks spinal nerve ligation-induced increases in spinal P-p38. Neurosci. Lett. 379:209–213.

Takeda, M., M. Takahashi, and S. Matsumoto. 2008. Contribution of activated interleukin receptors in trigeminal ganglion neurons to hyperalgesia via satellite glial interleukin-1beta paracrine mechanism. Brain Behav. Immun. 22:1016–1023.

Takeda, M., M. Takahashi, and S. Matsumoto. 2009. Contribution of the activation of satellite glia in sensory ganglia to pathological pain. Neurosci. Biobehav. Rev. 33:784–792.

Thakur, G. A., R. Tichkule, S. Bajaj, and A. Makriyannis. 2009. Latest advances in cannabinoid receptor agonists. Expert Opin. Ther. Pat. 19:1647–1673.

Thompson-Snipes, L., V. Dhar, M. W. Bond, T. R. Mosmann, K. W. Moore, and D. M. Rennick. 1991. Interleukin 10: a novel stimulatory factor for mast cells and their progenitors. J. Exp. Med. 173:507–510.

Toth, C. C., N. M. Jedrzejewski, C. L. Ellis, and W. H. Frey 2nd. 2010. Cannabinoid-mediated modulation of neuropathic pain and microglial accumulation in a model of murine type I diabetic peripheral neuropathic pain. Mol. Pain 6:16.

Treutwein, B., and H. Strasburger. 1999. Fitting the psychometric function. Percept. Psychophys. 61:87–106.

Tsuda, M., Y. Kohro, T. Yano, T. Tsujikawa, J. Kitano, H. Tozaki-Saitoh, S. Koyanagi, S. Ohdo, R. R. Ji, M. Salter, et al. 2011. JAK-STAT3 pathway regulates spinal astrocyte proliferation and neuropathic pain maintenance in rats. Brain 134:1127–1139.

Wallace, J. A., A. A. Romero, A. M. Gabaldon, V. A. Roe, S. L. Saavedra, and J. Lobner. 1996. Tyrosine hydroxylase-containing neurons in the spinal cord of the chicken. I. Development and analysis of catecholamine synthesis capabilities. Cell. Mol. Neurobiol. 16:625–648.

Walter, L., A. Franklin, A. Witting, C. Wade, Y. Xie, G. Kunos, K. Mackie, and N. Stella. 2003. Nonpsychotropic cannabinoid receptors regulate microglial cell migration. J. Neurosci. 23:1398–1405.

Watkins, L. R., J. Wieseler-Frank, M. R. Hutchinson, A. Ledeboer, L. Spataro, E. D. Milligan, E. M. Sloane, and S. F. Maier. 2007. Neuroimmune interactions and pain: the role of immune and glial cells. Pp. 393–411 *in* Ader, R., ed. Psychoneuroimmunology. Elsevier, Burlington, MA.

Wu, P., Y. I. Tarasenko, Y. Gu, L. Y. Huang, R. E. Coggeshall, and Y. Yu. 2002. Region-specific generation of cholinergic neurons from fetal human neural stem cells grafted in adult rat. Nat. Neurosci. 5:1271–1278.

Xu, J. T., W. J. Xin, X. H. Wei, C. Y. Wu, Y. X. Ge, Y. L. Liu, Y. Zang, T. Zhang, Y. Y. Li, and X. G. Liu. 2007. p38 activation in uninjured primary afferent neurons and in spinal microglia contributes to the development of neuropathic pain induced by selective motor fiber injury. Exp. Neurol. 204:355–365.

Yao, B. B., S. Mukherjee, Y. Fan, T. R. Garrison, A. V. Daza, G. K. Grayson, B. A. Hooker, M. J. Dart, J. P. Sullivan, and M. D. Meyer. 2006. In vitro pharmacological characterization of

 

AM1241: a protean agonist at the cannabinoid $CB_2$ receptor? Br. J. Pharmacol. 149:145–154.

Yao, B. B., G. Hsieh, A. V. Daza, Y. Fan, G. K. Grayson, T. R. Garrison, O. El Kouhen, B. A. Hooker, M. Pai, E. J. Wensink, et al. 2009. Characterization of a cannabinoid $CB_2$ receptor-selective agonist, A-836339 [2,2,3,3-tetramethyl-cyclopropanecarboxylic acid [3-(2-methoxy-ethyl)-4,5-dimethyl-3H-thiazol-(2Z)-ylidene]-amide], using in vitro pharmacological assays, in vivo pain models, and pharmacological magnetic resonance imaging. J. Pharmacol. Exp. Ther. 328:141–151.

Yasuo, S., M. Koch, H. Schmidt, S. Ziebell, J. Bojunga, G. Geisslinger, and H. W. Korf.2010. An endocannabinoid system is localized to the hypophysial pars tuberalis of Syrian hamsters and responds to photoperiodic changes. Cell Tissue Res. 340:127–136.

Zhang, J., C. Hoffert, H. K. Vu, T. Groblewski, S. Ahmad, and D. O'Donnell. 2003. Induction of $CB_2$ receptor expression in the rat spinal cord of neuropathic but not inflammatory chronic pain models. Eur. J. Neurosci. 17:2750–2754.

Zhuang, Z. Y., P. Gerner, C. J. Woolf, and R. R. Ji. 2005. ERK is sequentially activated in neurons, microglia, and astrocytes by spinal nerve ligation and contributes to mechanical allodynia in this neuropathic pain model. Pain 114: 149–159.

Zhuang, Z.-Y., Y. Kawasaki, P.-H. Tan, Y.-R. Wen, J. Huang, and R.-R. Ji. 2007. Role of the CX3CR1/p38 MAPK pathway in spinal microglia for the development of neuropathic pain following nerve injury-induced cleavage of fractalkine. Brain Behav. Immun. 21:642–651.

 